buildings

MDPI

Article

Dynamic Response of Transmission Tower-Line Systems Due to Ground Vibration Caused by High-Speed Trains

Guifeng Zhao, Meng Wang, Ying Liu and Meng Zhang *

School of Civil Engineering, Zhengzhou University, Zhengzhou 450001, China; gfzhao@zzu.edu.cn (G.Z.)
* Correspondence: zhangmeng@zzu.edu.cn

Abstract: With the continuous expansion of the scale of power grid and transportation infrastructure construction, the number of crossovers between transmission lines and high-speed railways continues to increase. At present, there is a lack of systematic research on the dynamic characteristics of transmission tower-line structures crossing high-speed railways under vehicle-induced ground vibration. This article focuses on the phenomenon of accidents such as line drops when crossing areas in recent years and establishes a high-speed train track foundation soil finite element model in ABAQUS that considers track irregularity. The three-dimensional vibration characteristics and attenuation law of train ground vibration are analyzed. Acceleration data for key points are also extracted. A separate finite element model of the transmission tower-line system is established in ANSYS, where acceleration is applied as an excitation to the transmission tower-line system, and the coupling effect between the tower and the line is considered to analyze its dynamic response. Subsequently, modal analysis is conducted on the tower-line system, providing the vibration modes and natural frequencies of the transmission tower-line structure. The effects of factors such as train speed, soil quality, and distance from the tower to the track on the dynamic response of the transmission tower-line system under vehicle-induced ground vibration are studied. The results show that the speed range (300 km/h–400 km/h) and track distance range (4.5 m–30 m) with the greatest impacts are obtained. The research results can provide a reference for the reasonable design of transmission tower-line systems in high-speed railway sections.

Keywords: high-speed train; ground vibration; transmission tower-line structure; numerical simulation; dynamic response

Citation: Zhao, G.; Wang, M.; Liu, Y.; Zhang, M. Dynamic Response of Transmission Tower-Line Systems Due to Ground Vibration Caused by High-Speed Trains. *Buildings* **2023**, *13*, 2884. https://doi.org/10.3390/buildings13112884

Academic Editors: Carmelo Gentile and Fabio Rizzo

Received: 4 August 2023
Revised: 13 November 2023
Accepted: 16 November 2023
Published: 18 November 2023

1. Introduction

Power grid systems and railway systems are important material foundations of modern society and an important part of lifeline engineering systems. In the past 20 years, high-speed railways have developed rapidly in many countries due to their advantages of safety, efficiency, low energy consumption, and large transportation capacity. At the same time, high-voltage overhead transmission, as the main mode of power supply in countries around the world, has also developed significantly in the past few decades. With the continuous increase in social electricity demand and transportation demand, the power grid and transportation infrastructure are constantly being upgraded and constructed, which brings about the inevitable problem of crossings of transmission tower-line systems and high-speed railways (Figure 1). In the crossover area of the two, once an accident, such as disconnection, string drop, or even tower collapse, occurs, it may cause a large-scale power supply interruption. Therefore, ensuring the long-term safe operation of the power grid system and the railway system across both sections is a matter of great concern to both the power sector and the railway sector.

Figure 1. Cases of overhead transmission lines crossing high-speed railways.

With the increase in high-speed railway construction mileage and the improvement of high-speed train operating speed [1], the environmental vibration problem caused by high-speed trains has become increasingly prominent. At present, many scholars have conducted relatively comprehensive research on the generation mechanism of ground vibration caused by high-speed trains and the law of vibration propagation. For the generation mechanism of vehicle-induced ground vibration, the research mainly focuses on three aspects: theoretical analysis models, field tests, and finite element numerical simulations. Typical theoretical analysis models include the Winkler foundation beam theory [2], the Timoshenko elastic foundation beam model [3], and the basic model of wheel–rail interaction considering unsprung mass and track stiffness [4]. Because the ground vibration caused by trains usually propagates near the surface [5], research mainly focuses on the propagation law of ground vibration, including the simulation of roadbeds and ground [6], the simulation of track irregularity [7], and the theoretical analysis of large coupling vibration problems [8]. In recent years, researchers have studied the problems of vehicle-induced ground vibration using finite element numerical simulation and field test methods. For example, Xia et al. [9] established a comprehensive model considering train-track-foundation dynamic interactions. Factors such as the quasistatic axle load and dynamic excitation between the wheel and rail are analyzed. The results show that the ground vibration characteristics are closely related to the train speed and soil characteristics. With increasing track distance, the ground acceleration tends to decrease. Erkal et al. [10] measured triaxial vibrations of road and rail traffic on and around a typical residential masonry building in Istanbul and its response to adjacent ground-born vibrations through numerical modeling. The results show that train-induced vibrations caused the walls of the building to experience tensile stresses up to 23% of the masonry tensile strength. Motazedian et al. [11] found that the durations and amplitudes of the train-induced seismic waves at soil sites increased dramatically compared to those at the reference bedrock site. On the other hand, very large soil amplifications have been observed based on local earthquake recordings, with a very different source mechanism than train-induced seismic waves. Niu et al. [12] studied the ground vibration caused by the operation of the Datong–Xi'an high-speed railway through field tests. The results show that the ground vibration caused by a high-speed train is a periodic excitation, and the vertical vibration acceleration of the ground decreases with increasing distance from the vibration source.

Because the vibration caused by trains will be transmitted to the surrounding soil layer through the track, roadbed, etc., and then cause secondary vibration of the adjacent structures, some scholars have also conducted studies on the dynamic response of such structures under the action of high-speed trains. Chen et al. [13] experimentally studied the site dynamic response of a bridge and its surrounding environment on the Wuhan–Guangzhou high-speed railway. The results show that the vertical vibration acceleration of the bridge is generally between 0.07 and 0.25 m/s^2. With increasing train speed, the ground vibration gradually increases. Hesami et al. [14] used a two-dimensional finite element method to analyze the influence of train vibration on residential buildings near the

Qaemshahr railway. The train–ground dynamic model is preliminarily verified by the measured data. The results show that the vibration level decreases significantly with increasing distance from the track centerline to the building. Zhou et al. [15] sampled vibration data from the proposed site near the railway, and the measured ground acceleration was used as the excitation for the proposed building. The law of some trains' impact on the vibration of nearby buildings was obtained. Erkan et al. [16] studied the ground vibration caused by high-speed trains and its impact on surrounding residential areas through a large amount of field work and many field measurements in Türkiye. The above studies mainly focus on the impact of ground vibration caused by high-speed trains on adjacent high-rise buildings, bridge structures, and residential areas.

In the study of train vibration, one of the very important factors is the excitation source target interaction system. When an excitation source (such as mechanical vibration or vehicle dynamic load) acts on the ground, the soil will generate and transmit excitation energy and interact with the target structure. Conversely, the response of the structure, such as vibration and dynamic forces, will also be transmitted along the soil, affecting the source of motivation. One important method is to use transfer functions to analyze the impact of excitation sources on ground motion [17] and, finally, the impact on the analyzed object. Due to the high stability requirements of the large Hadron collider (HL-LHC) for the orbit, Schaumann et al. [18] conducted some research to characterize the actual ground motion in the large Hadron collider tunnel and summarized the observations made on the LHC beams. Farahani et al. [19] developed a numerical model based on the modal analysis results of buildings to address the impact of vibrations caused by trains on residents in the vicinity of railway lines. The double confirmation analysis method is used to identify the modal parameters of buildings: obtain the transfer function through the dynamic response of modal analysis; reproduce the vibration acceleration of different floors of the building from on-site measurement records; and apply it to the building foundation.

Considering the large-span and high-rise structural characteristics of high-voltage overhead transmission tower-line systems, wind load is usually the dominant load. A large number of studies have been conducted in such areas, including the design wind loads [20], wind-induced vibration [21–23], and galloping [24,25] of transmission tower-line systems, which provide effective technical support for the rational design and maintenance of high-voltage transmission tower-line systems. In fact, the transmission tower-line system across the high-speed railway will also be affected by the environmental vibration caused by high-speed trains. Taking China as an example, Feng et al. [26] reported that with the continuous development of power transmission capacity and railway transportation capacity, the proportion of the crossing of transmission tower-line systems and high-speed railways will continue to increase. Yin et al. [27] numerically studied the dynamic response of transmission lines under the action of high-speed trains and verified it by field tests. Zhang et al. [28] and Liu [29] analyzed the transient force and typical dynamic response of an overhead transmission tower-line structure under the action of high-speed train-induced wind. The results show that when the train passes through the overhead transmission tower-line structure, the ultimate force of the transmission line has a significant quadratic function relationship with the train speed.

In summary, the phenomenon of crossings between overhead transmission tower-line systems and high-speed railways will continue to increase in the future, but there is currently a lack of systematic research on the dynamic response of transmission tower-line structures across high-speed railways under vehicle-induced ground vibration. To this end, a high-speed train track foundation soil finite element model is established in ABAQUS that considers track irregularity. The three-dimensional vibration characteristics and attenuation law of train ground vibration are analyzed. A separate finite element model of the transmission tower-line system was established in ANSYS. Factors such as different soil qualities, different train speeds, and different distances to the track are discussed. This study is expected to provide a reference for the rational design and daily maintenance of transmission tower-line systems across high-speed railways.

2. Establishment and Verification of the Finite Element Model

To study the effect of ground vibration caused by high-speed trains on the transmission tower-line system, the acceleration time history of the ground surface during the process of the high-speed train passing through the transmission tower-line system was obtained by a numerical simulation method, and then it was used to perform a dynamic analysis of the transmission tower-line system.

2.1. Establishment and Verification of the Train-Track-Foundation-Soil Coupling Model

This section mainly focuses on the theoretical methods and parameters related to the establishment of the finite element model of the train-track-foundation soil. Because ABAQUS 2021 can better simulate the nonlinear contact problem between wheels and rails and the explicit integration algorithm in ABAQUS can solve highly nonlinear quasistatic problems, complex contact problems, and high-speed dynamic loads, the explicit dynamic integration method (ABAQUS/Explicit) is used in this study. A schematic diagram of the model is shown in Figure 2.

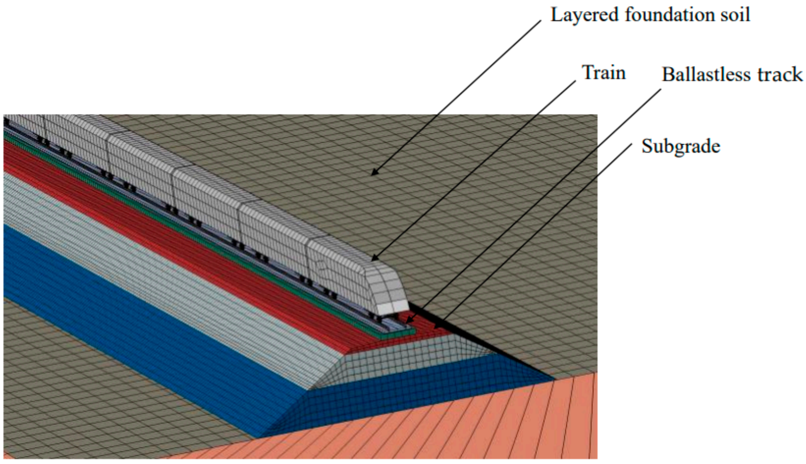

Figure 2. Train-track-foundation-soil coupling model.

2.1.1. Model of the Train

The motion of the vehicle system in the vertical longitudinal plane can be considered a multirigid body system, and the vehicle body model with a secondary spring mass is used. The following assumptions are used for the model [2]. Only the wheel–rail vertical dynamic effect is considered in the model. The car body, bogie, and wheelset are regarded as rigid bodies, and the influence of the deformation of these components on the overall model is not considered. The wheelset and the bogie are connected by a series of springs and damping elements; the connection between the bogie and the car body is composed of a second series of springs and damping elements. The masses of the car body, bogie, and wheelset are simplified as centralized mass considerations. The single vehicle part of the overall model has 16 degrees of freedom, such as the ups and downs of the car body and the three-way nodding, the ups and downs of the front and rear bogies and the three-way nodding, and the ups and downs of the four-wheel sets.

Taking an ICE3-type train [30] as an example, a finite element model of train-track-foundation-soil is established to simulate the propagation and attenuation of vibration waves generated by wheel–rail action in the soil layer. The driving distance is 444 m. The speed of the train selected in this section is 250 km/h. The schematic diagram is shown in Figure 3. In this figure, M_c and J_c are the mass and moment of inertia of the car body, respectively; M_t and J_t are the mass and moment of inertia of the bogie, respectively; M_ω is the quality of the wheelset; K_{s1} and C_{s1} are the primary suspension mass and damping, respectively; and K_{s2} and C_{s2} are the suspension mass and damping of the secondary series, respectively. The above parameters and other geometric parameters are listed in Table 1.

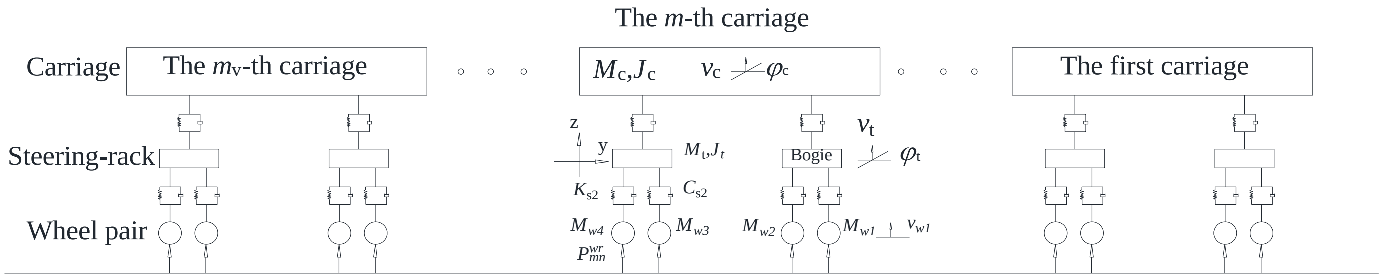

Figure 3. Secondary suspension vehicle model and parameters.

Table 1. Mechanical and geometric parameters of train vehicles.

Vehicle Parameters	Size
$M_c(\mathrm{kg})$	47,900
$J_c\left(\mathrm{kg/m^2}\right)$	Lateral is 8.224×10^6 Vertical is 8.232×10^6 Longitudinal is 2.751×10^5
$M_t(\mathrm{kg})$	1381
$J_t\left(\mathrm{kg/m^2}\right)$	Lateral is 1695 Vertical is 2844 Longitudinal is 1378
$M_\omega(\mathrm{kg})$	1400
$K_{s1}(\mathrm{N/m})$	1.87×10^6
$C_{s1}(\mathrm{N \cdot s/m})$	5×10^5
$K_{s2}(\mathrm{N/m})$	1.72×10^5
$C_{s2}(\mathrm{N \cdot s/m})$	1.92×10^5
Tire size (m)	0.46
Distance from coupler to coupler (m)	2.50
Wheel base $2d$ (m)	2.50

2.1.2. Train-Track Model

The CRTS I-type ballastless track is adopted to build the train-track model. The track components include steel rails, sleepers, elastic fasteners, track slabs, CAE mortar filling layers, and concrete bases. In this paper, a simplified track model is used, and its cross-section is shown in Figure 4. The gauge of the two rails is 1.435 m, and the track fastener spacing is 0.6 m. The parameters of the sleeper, track slab, CAE mortar, and concrete base are shown in Table 2.

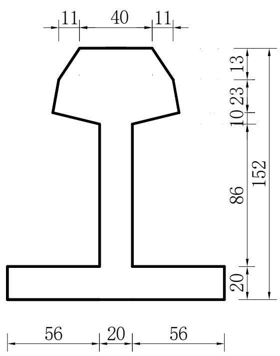

(**a**)

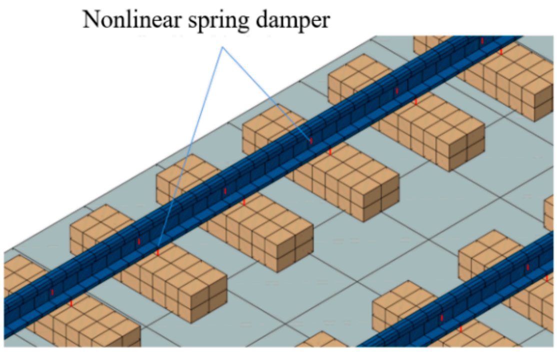

(**b**)

Figure 4. Details of the track section. (**a**) Simplified track cross-section size diagram (mm). (**b**) Finite element model of ballastless track.

Table 2. Parameters of the track structure.

Structure Layer Name	Width (m)	Depth (m)
Track board	2.4	0.20
CA mortar bed	2.4	0.05
Concrete base	3	0.30
Rail bearing	0.25	0.16

To prevent the occurrence of an hourglass phenomenon where the unit lacks stiffness and cannot resist deformation, each unit adopts an hourglass control. The actual connection between the rail and the sleeper is a fastener, which is used to limit the vertical displacement of the rail through tension. Therefore, in ABAQUS, the fastener is simulated with a nonlinear spring-damper element that can only be tensioned, as shown in Figure 4b. The actual track board is connected by many standard-length track boards, but considering the strong longitudinal connection between the track boards, this model will not model the standard track board and then consider the longitudinal connection but, instead, will model the overall structure of the track board and other structures in the longitudinal direction. The convex retaining platform and other lateral limiting devices that play a longitudinal limiting role will not be physically modeled, and their limiting effect will be replaced by specifying boundary conditions for the track structure. The material parameters of the track structure are listed in Table 3.

Table 3. Track structure material parameters.

Structure Layer Name	Density (kg/m^3)	Elastic Modulus (Pa)	Poisson's Ratio
Steel rail	7800	2.06×10^{11}	0.25
Rail bearing	2500	3.60×10^{10}	0.20
Track board	2600	3.50×10^{10}	0.17
CA mortar bed	1800	9.20×10^{6}	0.40
Concrete base	2500	2.40×10^{10}	0.20

2.1.3. Track Irregularities

Track irregularity refers to the deviation between the track contact surface used to support and guide the wheels along the length direction of the track and the theoretical smooth track, which is the main excitation that causes the change in the wheel–rail action and then the coupled vibration of the entire train-track-foundation-soil system. The track irregularity spectrum of each country is divided into two levels: low interference and high interference. The low-interference level is suitable for high-speed railways above 250 km/h. For China's trunk railways, the more typical statistical spectrum functions that can characterize the irregularity characteristics include various speed levels, such as 120 km/h, 160 km/h, and 200 km/h [31].

For the high-speed train considered in this study, the above various track irregularity spectra cannot be better adapted to the working conditions of this study. To address this issue, Xu et al. [32] compared and analyzed the track irregularity spectrum at all levels and noted that the distribution of the low-interference track irregularity spectrum in Germany is similar to the standard spectrum of the 200 km/h speed-up line in China and can be used in the speed-up line spectrum in China. Additionally, the simulated power spectral density function of the track irregularity of the 350 km/h high-speed rail line at the design speed is also obtained based on the above track spectral density function and the sample data of the Shanghai–Nanjing passenger dedicated line. In view of the need to predict the impact of higher train speeds on the ground vibration caused by high-speed trains, the track irregularity power spectral density function used in this study is the German low-interference track irregularity spectrum suitable for speeds greater than 250 km/h and the simulated irregularity spectrum corresponding to a speed of 350 km/h [32].

Due to the unevenness of the track level and other directions, it contributes less to the excitation between the wheel and rail [33], so, in this study, only the level track irregularity is considered. Using $S_v(\Omega)d\Omega = S_v(f)df$, the spectral functions of the German low-interference high–low irregularity spectrum, and the 350 km/h high–low irregularity spectrum varying with time and frequency can be obtained as follows:

(1) German low-interference track irregularity spectrum:

$$S_v(f) = S_v(\frac{2\pi f}{v}) \cdot \frac{2\pi}{v} = \frac{A_v \cdot f_c^2 v}{2\pi(f^2 + f_r^2)(f^2 + f_c^2)} \tag{1}$$

where f_r is the spatial cutoff frequency, Ω_r is the corresponding time truncation frequency ($f_r = v\Omega_r/2\pi$), f_c is the spatial cutoff frequency, and Ω_c is the corresponding time truncation frequency ($f_c = v\Omega_c/2\pi$).

(2) Simulated track irregularity spectrum for 350 km/h [32]:

$$S_v(f) = \frac{a(f^2v^{-3}) + b(fv^{-2})}{(1 + bfv^{-1} + cf^3v^{-3})} \tag{2}$$

With the help of the MATLAB program and inverse Fourier transform method, the discrete data of the amplitude of track irregularity changing with time can be obtained based on the above-mentioned power spectral density function that changes with time and frequency. The results are shown in Figure 5a,b. In comparison with the current literature, it is found that the simulated amplitude of the track irregularities according to the German low-interference spectrum is very close to the data calculated by Chen et al. [34], and the amplitude of the track irregularities obtained by the Shanghai–Nanjing 350 km/h spectrum is almost the same as the amplitude in the literature [32]. To verify the precision of the simulated method in this study, the simulated results and analytical values of the two kinds of irregularity spectra are also compared, as shown in Figure 6.

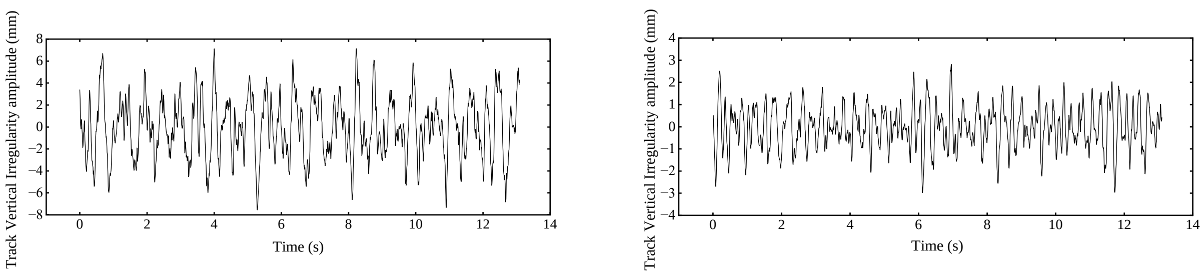

(**a**) (**b**)

Figure 5. Vertical irregularity amplitude simulation time series. (**a**) Simulated time series of low-interference high–low irregularity amplitude in Germany. (**b**) The simulated 350 km/h track irregularity amplitude time series.

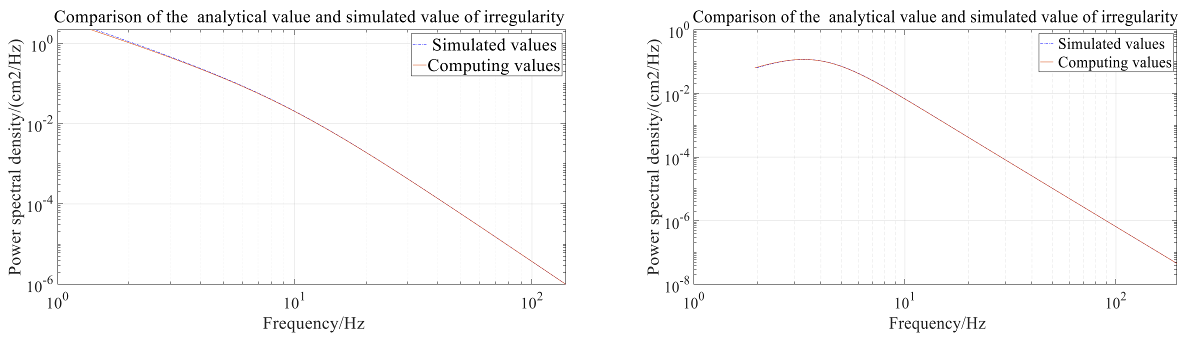

(**a**) (**b**)

Figure 6. Comparison of the simulated and analytical values of the irregularity power spectrum. (**a**) The spectrum of German low interference. (**b**) The spectrum of 350 km/h.

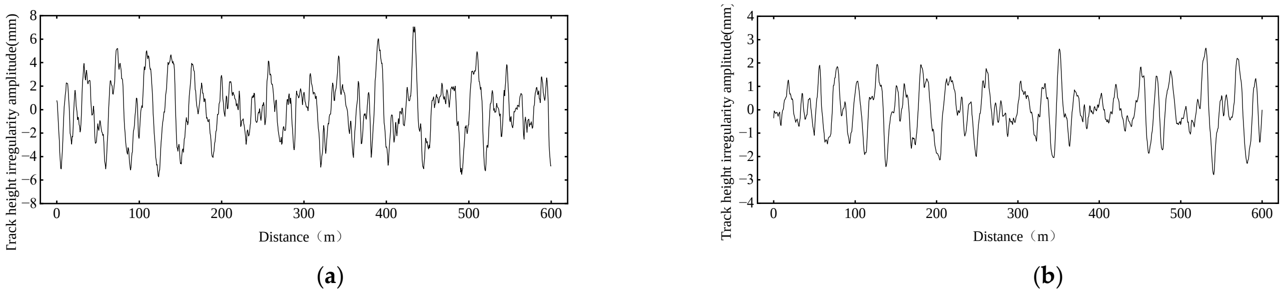

Figure 7. The relationship between the amplitude vertical irregularity and the forward distance of the train. (**a**) The relationship between the amplitude of German low-interference vertical irregularity and the forward distance of the train. (**b**) The relationship between the amplitude of 350 km/h irregularity amplitude and the forward distance of the train.

2.1.4. Subgrade and Foundation Soil Model

(1) Subgrade model parameters

According to the "Code for Design of High-speed Railway" [35], the subgrade section of the model in this study is based on the standard cross-sectional dimensions of single-line embankments for medium-ballasted tracks, as shown in Figure 8. The specification stipulates that the surface of the subgrade should be filled with graded gravel, and considering the large deformation of the subgrade, for the accuracy of the model, the Drucker–Prager plastic material constitutive model is used for each subgrade. The parameters of each layer of the roadbed structure are listed in Table 4.

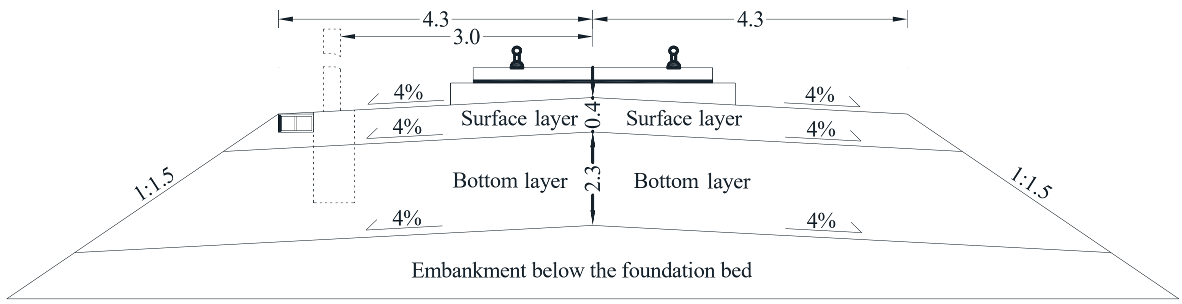

Figure 8. Single-line embankment ballastless track standard cross-section diagram.

Table 4. Geometric and mechanical parameters of each layer of the subgrade structure.

Names of Each Foundation Bed	Thickness (m)	Dynamic Elastic Modulus (MPa)	Poisson's Ratio	Density (kg/m^3)	Cohesion (Pa)	Internal Friction Angle (°)	Damping Ratio
Surface layer of foundation bed	0.4	120	0.3	2184	7×10^4	27	0.045
Bottom layer of subgrade bed	2.3	70	0.3	1939	5×10^4	23	0.039
Embankment	3.6	50	0.35	1837	4×10^4	20	0.035

The triaxial test parameters that need to be input into the definition of the Drucker–Prager plastic material constitutive model are obtained by the following formula:

$$\tan\beta = \frac{6\sin\varphi}{3-\sin\varphi} \tag{3}$$

$$K = \frac{3-\sin\varphi}{3+\sin\varphi} \tag{4}$$

$$\sigma_c = \frac{2c\cos\varphi}{1-\sin\varphi} \tag{5}$$

where φ is the friction angle in the Coulomb constitutive model (see Table 4), c is cohesion, K is the flow stress ratio ($0.078 \leq K \leq 1$), and the plastic parameters needed for each layer of the model subgrade structure are shown in Table 5.

Table 5. Drucker–Prager parameters for each layer of the subgrade structure.

Name of the Subgrade Structure of Each Layer	Angle of Friction (°)	Flow Stress Ratio K)	Expansion Angle (°)	Compression Yield Stress (Pa)	Absolute Plastic Strain
Surface layer of foundation bed	27	0.855	0	177847.90	0
Bottom foundation bed	23	0.876	0	122247.00	0
Embankment	20	0.892	0	95136.97	0

(2) Parameters of the foundation soil model

Usually, the loading speed and different strain levels on the soil will directly lead to the state of elasticity, elastoplasticness, or failure of the soil [36]. The dynamic strain of soil caused by rail transit is generally very small, and generally less than 1×10^{-5}. At this time, the soil is almost completely in the elastic stage. Therefore, the following assumptions [2] are adopted for the soil model in this study. The foundation soil is assumed to be a layered elastic body, and the material of each layer of soil is consistent and simplified as isotropic. The atomic and molecular motions and internal pores of soil particles in the soil are not considered, and continuous functions can be used to describe the changing laws of physical quantities such as soil stress, deformation, and displacement. The initial stress of the soil is neglected.

According to the literature [34], the soil below the subgrade is divided into two types: soft soil and hard soil. Among them, the soft soil is analyzed by using a representative three-layer soil in a soft soil area in Shanghai. The distinction between soft and hard soil is based on the shear wave velocity of the soil. Both soft and hard soil materials adopt linear elastic constitutive models. In this study, the shear wave velocity of the soil is calculated by using the following formula:

$$V_s = \sqrt{\frac{E}{2\rho(1+\mu)}} \tag{6}$$

where E is the elastic modulus of the soil, μ is Poisson's ratio, and ρ is the soil density. The material parameters of soft and hard soil and the shear wave velocity obtained from the above formula are shown in Table 6.

The size of the foundation soil along the length of the train is 600 m, the length of the foundation soil in the vertical direction of the train is 150 m, and the thickness of the entire foundation soil is 60 m. In addition, since the vibration wave will produce a reflection effect when it propagates to the finite element boundary, the calculation accuracy of the vibration wave will be greatly reduced. To reduce this effect, the infinite element boundary is set in the INP file of ABAQUS for the surrounding and bottom of the foundation soil. The model is shown in Figure 9. The infinite part of the Earth's foundation is equivalent to a boundary. For the boundary at the bottom of the foundation, considering a certain depth, the influence of boundary impedance and scattering characteristics is very small, and the bottom belongs to the rock layer, so the bottom of the model adopts consolidation constraints. Furthermore, it should be noted that since the boundary of the foundation soil model has been simulated using infinite elements, the roadbed structure will not be placed at the center of the foundation soil surface but on the side close to the foundation soil surface to extract the response of surface points within the range of 4.5~49.5 m from the track center.

Table 6. Geometric and material parameters of soft and hard soil layers.

Soil Type	Name of Each Layer of Soil	Thickness (m)	Dynamic Elastic Modulus (MPa)	Poisson's Ratio	Shear Wave Velocity (m/s)	Density (kg/m^3)	Damping Ratio
Soft soil	Silty clay	6	30	0.290	78.27	1898	0.050
	Silt clay	9	14	0.300	56.21	1704	0.050
	Sandy silt	24	74	0.310	123.66	1847	0.050
	Uniform elastic half-space soil layer	21	141	0.330	167.03	1900	0.023
Hard soil	Silty clay	6	124	0.302	158.40	1898	0.020
	Silt clay	9	111	0.310	157.82	1704	0.020
	Sandy silt	24	159	0.318	180.83	1847	0.020
	Uniform elastic half-space soil layer	21	141	0.330	167.03	1900	0.020

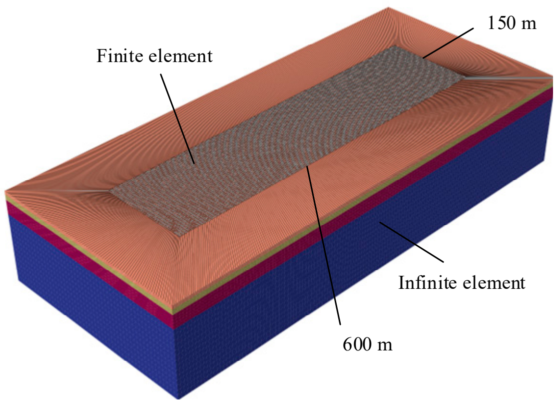

Figure 9. Schematic diagram of the foundation soil model with an infinite element boundary.

2.1.5. Calculation of Damping

Damping in ABAQUS/Explicit is mainly defined by the Rayleigh damping option, which can be determined by:

$$[C] = \alpha[M] + \beta[K] \tag{7}$$

where α, β is the proportionality constant related to the natural circular frequency of the structure and the damping ratio of the material [37], which can be determined by the following formula:

$$\begin{cases} \alpha = \frac{2(\xi_i\omega_j - \xi_j\omega_i)\omega_i\omega_j}{(\omega_j+\omega_i)(\omega_j-\omega_i)} \\ \beta = \frac{2(\xi_j\omega_j - \xi_i\omega_i)}{(\omega_j+\omega_i)(\omega_j-\omega_i)} \end{cases} \tag{8}$$

where ω_i and ω_j are the ith- and jth-order natural frequencies, respectively, and ξ_i and ξ_j are the damping ratios corresponding to the ith- and jth-order natural frequencies, respectively. In practical applications, due to the difficulty in determining the variation of ξ_i and ξ_j with natural frequencies, they are usually simplified as $\xi_i = \xi_j = \xi$. The Rayleigh damping can be obtained from Equations (7) and (9):

$$\begin{cases} \alpha = \frac{2\xi\omega_i\omega_j}{(\omega_j+\omega_i)} \\ \beta = \frac{2\xi}{(\omega_j+\omega_i)} \end{cases} \tag{9}$$

The entire foundation soil, including the subgrade section, is subjected to modal analysis, the calculation efficiency and model accuracy are considered comprehensively, and only the first 30 orders of natural circle frequencies of the foundation soil of different soil qualities are extracted. Since the vertical vibration of the foundation soil is the main concern in this study, only the participation coefficient of each order frequency in the vertical formation is extracted, as shown in Figure 10.

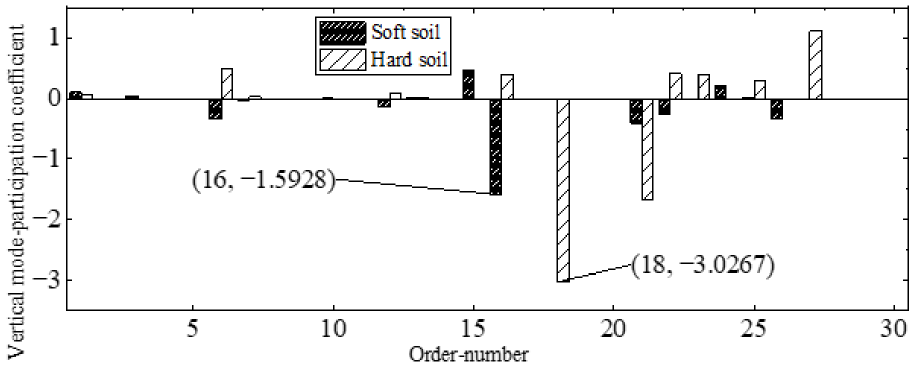

Figure 10. Each order natural frequency vertical mode-participation coefficient diagram.

Figure 10 indicates that the participation coefficient of the 16th-order natural frequency of soft soil is the largest in the vertical formation, which is 1.5928, and the participation coefficient of the 18th-order natural frequency of hard soil is the largest in the vertical formation, which is 3.0267. Therefore, the 16th-order natural frequency of soil and the 18th-order natural frequency of hard soil are selected as ω_j, and the first-order natural frequencies of soft and hard soils are selected as ω_i in Formulas (9) to calculate the Rayleigh damping coefficient. The calculated coefficients α and β are shown in Table 7.

Table 7. Rayleigh damping coefficient table of soft and hard soil.

Soil Quality	Name	ξ	ω_i	ω_j	α	β
Soft soil	Surface layer of foundation bed	0.045	3.0536	3.9663	0.1553	0.0128
	Bottom layer of subgrade bed	0.039	3.0536	3.9663	0.1346	0.0111
	Embankment	0.035	3.0536	3.9663	0.1208	0.0100
	Silty clay	0.050	3.0536	3.9663	0.1725	0.0142
	Silt clay	0.050	3.0536	3.9663	0.1725	0.0142
	Sandy silt	0.050	3.0536	3.9663	0.1725	0.0142
	Uniform elastic half-space soil layer	0.023	3.0536	3.9663	0.0794	0.0066
Hard soil	Surface layer of foundation bed	0.045	3.9628	6.3627	0.2198	0.0087
	Bottom layer of subgrade bed	0.039	3.9628	6.3627	0.1905	0.0076
	Embankment	0.035	3.9628	6.3627	0.1709	0.0068
	Silty clay	0.020	3.9628	6.3627	0.0977	0.0039
	Silt clay	0.020	3.9628	6.3627	0.0977	0.0039
	Sandy silt	0.020	3.9628	6.3627	0.0977	0.0039
	Uniform elastic half-space soil layer	0.020	3.9628	6.3627	0.0977	0.0039

2.1.6. Wheel–Rail Contact and Track-Subgrade Connection

Regarding the contact relationship between the wheel and rail, the typical Hertz nonlinear elastic contact theory is adopted in this study. The contact elastic action between the wheel and rail is simplified as a linear spring and is defined by the Hertz contact stiffness.

$$k_H = \frac{dP}{d\Delta Z} = \frac{3}{2G}P^{1/3} \quad (10)$$

where the wheel–rail contact constant of the tapered tread is , and R is the wheel radius, with a value of 0.46 m in this study, so $G = 5.131 \times 10^{-8}$.

In ABAQUS/Explicit, nonlinear elastic contact is mainly achieved by setting the proportional relationship between contact pressure and interference according to Formula (3), which is set in ABAQUS/Explicit as the relationship between "softening" pressure and interference that conforms to the exponential law, as shown in Figure 11.

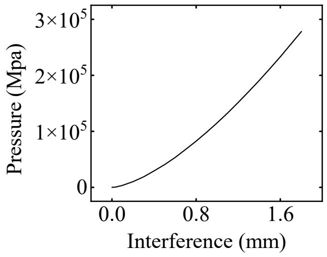

Figure 11. Pressure–interference diagram defined in ABAQUS/Explicit.

Considering that the sliding between the base of the track and the foundation is relatively small, the TIE connection is used. The so-called TIE connection binds the two surfaces that are in contact with each other. This processing method can better meet the deformation co-ordination relationship between the various parts of the track structure with a lower computational cost than the specified contact connection method.

2.1.7. Verification of the Finite Element Model

To verify the correctness of the model in this study, the same foundation soil size as in refs. [30,38] is used, soft soil type foundation soil is selected, and the train speed is 250 km/h. Considering the influence of the unevenness of the track on the ground vibration caused by the vehicle, the calculation and extraction are located in the middle of the model along the running direction of the track, and the distance from the vertical direction of the track is calculated and extracted. The monitoring points are demonstrated in Figure 12. Figure 13 shows a comparison of the vertical acceleration time history and the amplitude frequency between the present results and the results in ref. [30] at monitoring points of 4.5 m, 19.5 m, and 49.5 m.

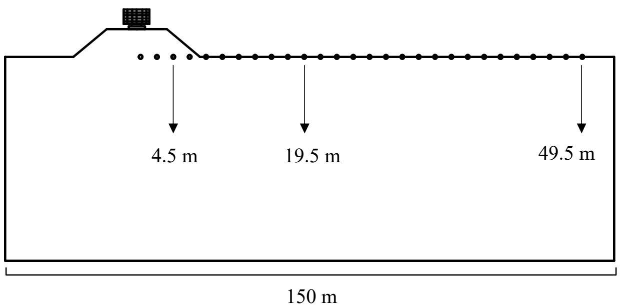

Figure 12. Train-track-foundation-soil coupling model monitoring point diagram.

As demonstrated in Figure 13, the present results are in good agreement with the results of ref. [30], and all of them are dominated by low-frequency responses, which is mainly due to the strong suppression of high-frequency vibrations by soft soils. To further verify the model in this study, working conditions (i.e., soft soil foundation and train speed 260 km/h) similar to those in ref. [38] are used to perform the analysis. The comparison of acceleration and displacement amplitude between the present study and the results of ref. [38] are listed in Table 8.

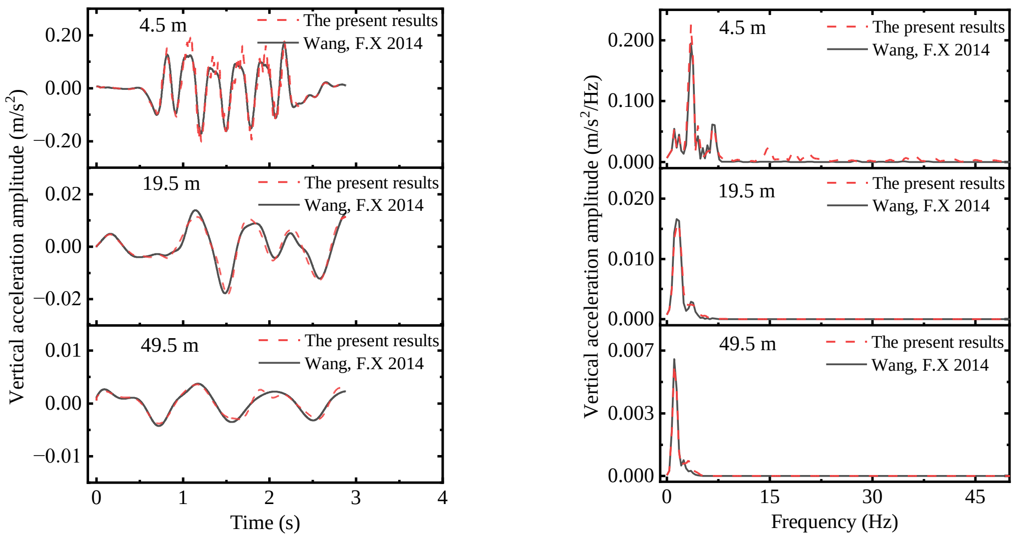

(**a**) (**b**)

Figure 13. Comparison of vertical acceleration between the present results and the results in ref. [30]. (**a**) Vertical acceleration time history diagram. (**b**) Vertical acceleration amplitude frequency diagram.

Table 8. Comparison of acceleration and displacement amplitude between the present results and the results in ref. [38].

Data Sources	Monitoring Point	Vertical Acceleration Amplitude (m/s^2)	Vertical Displacement Amplitude (mm)
Results of ref. [38]	Ground surface at a distance of 5 m from the track	0.15	1.3
Present results	Ground surface at a distance of 4.5 m from the track	0.18	1.4

Table 8 shows that both the acceleration amplitude and displacement amplitude results calculated by using the present model are close to the results in ref. [39]. In summary, the finite element model established in this study is reliable and can be used to simulate more engineering cases.

2.2. Analysis of Three-Dimensional Vibration Characteristics and Attenuation Law

To obtain the general vibration characteristics and attenuation law of the coupling model of train-track-foundation soil during train operation, this section selects a speed of 250 km/h, considers the high and low irregularity of the track (using German low-interference high- and low-irregularity spectrum), and analyzes the conditions when the foundation soil is soft soil. To reflect the variation in foundation soil vibration with the entire process of train travel, a series of monitoring points were selected in the middle of the entire soil model train travel direction at different distances perpendicular to the track direction, as shown in Figure 12. For the convenience of description, the direction perpendicular to the train travel is defined as the X direction, the vertical vibration direction is defined as the Z direction, and the train travel direction is defined as the Y direction. By extracting triaxial acceleration time history data at various monitoring points located at different distances (1.8 m–90 m) perpendicular to the track and plotting a triaxial acceleration–distance–amplitude waterfall chart, the vibration response characteristics of each measurement point can be obtained.

Figure 14 shows the triaxial acceleration time history curve at a distance of 1.8 m–90 m from the track center on the ground surface. The time history curves of the triaxial acceleration can better reflect the entire process of the train passing through the monitoring points. The change in acceleration amplitude in the middle part of the entire time domain can well reflect the process of the train passing through, and, due to the presence of wheels, the peaks in the triaxial acceleration time domain graph all exhibit periodic changes. The amplitude of the acceleration dynamic response in all three directions shows a decreasing trend as the distance to the center of the track increases, and the attenuation speed is first fast and then slow. At the same time, the periodic phenomenon of wave peaks caused by the wheel set effect gradually weakens as the distance to the track increases.

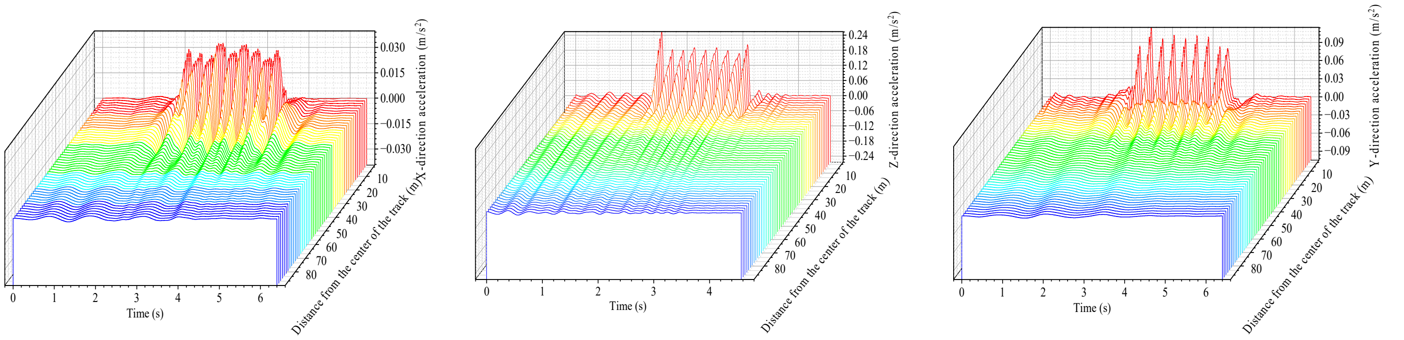

(**a**) (**b**) (**c**)

Figure 14. Time history of ground acceleration at different distances from the center of the track. (**a**) Time history of ground X-direction acceleration at different distances from the center of the track. (**b**) Time history of ground Z-direction acceleration at different distances from the center of the track. (**c**) Time history of ground Y-direction acceleration at different distances from the center of the track.

In terms of the amplitude of triaxial acceleration, the Z direction is the largest, followed by the Y direction, and the X direction is the smallest. In terms of the overall attenuation speed, the Z direction is the fastest, followed by the Y direction, and the X direction is the slowest. In addition, the attenuation speed of the triaxial acceleration also exhibits different patterns at different distances from the track: the attenuation speed of the Y and Z acceleration amplitudes within 20 m of the track center is significantly greater than that of the X direction, and the attenuation speed of the Z acceleration outside 20 m of the track sharply decreases and tends to flatten out. Within 20–40 m of the track, the attenuation speed of the Y direction acceleration is the highest among the three directions, while the attenuation speed of the X-direction acceleration is the slowest compared to the other two directions, and a rapid decrease in attenuation speed only occurs at approximately 40 m to the center of the track.

To study the vibration characteristics of the foundation soil in more detail, monitoring points were selected at the center of the roadbed surface and at distances of 4.5 m, 19.5 m, and 49.5 m from the track center, and their dynamic response data were analyzed in the time and frequency domains.

Figure 15 shows the triaxial acceleration time history and amplitude frequency at the center of the roadbed surface. Due to the proximity of the roadbed surface to the wheel–rail contact position, the amplitude of the triaxial acceleration dynamic response is significantly greater than that of the foundation soil surface. In addition, from the amplitude frequency of the triaxial acceleration at the roadbed, it can be seen that the frequency bandwidth of the roadbed surface is significantly greater than that of the foundation soil surface, and the triaxial acceleration frequency is significantly concentrated in the higher frequency range, indicating that the roadbed structure has a strong inhibitory effect on the vibration at higher frequencies.

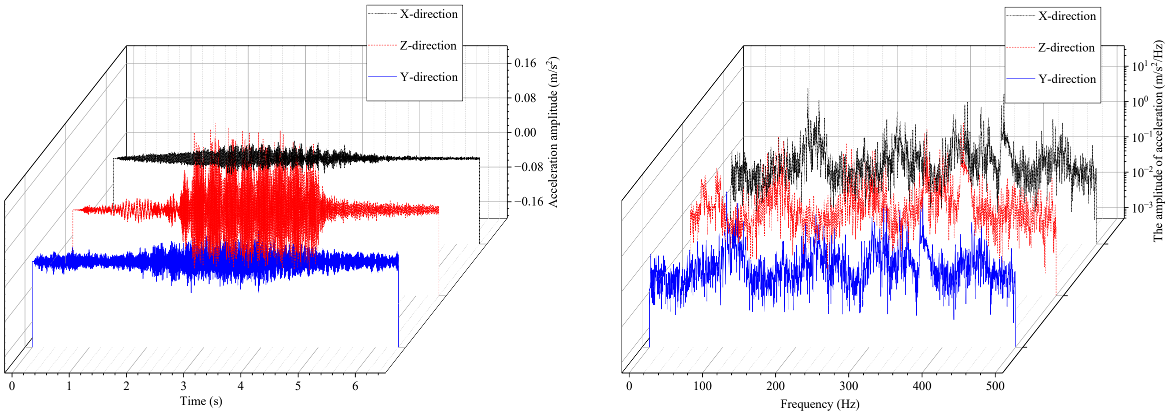

(**a**) (**b**)

Figure 15. Three-dimensional dynamic response diagram of the roadbed surface. (**a**) The acceleration time history. (**b**) Amplitude frequency of the acceleration.

Figure 16 shows the time history and amplitude frequency of the triaxial acceleration on the foundation soil surface at distances of 4.5 m, 19.5 m, and 49.5 m from the center of the track. To provide a detailed explanation of the ground surface vibration characteristics and attenuation law, the following are described separately in terms of the time and frequency domains.

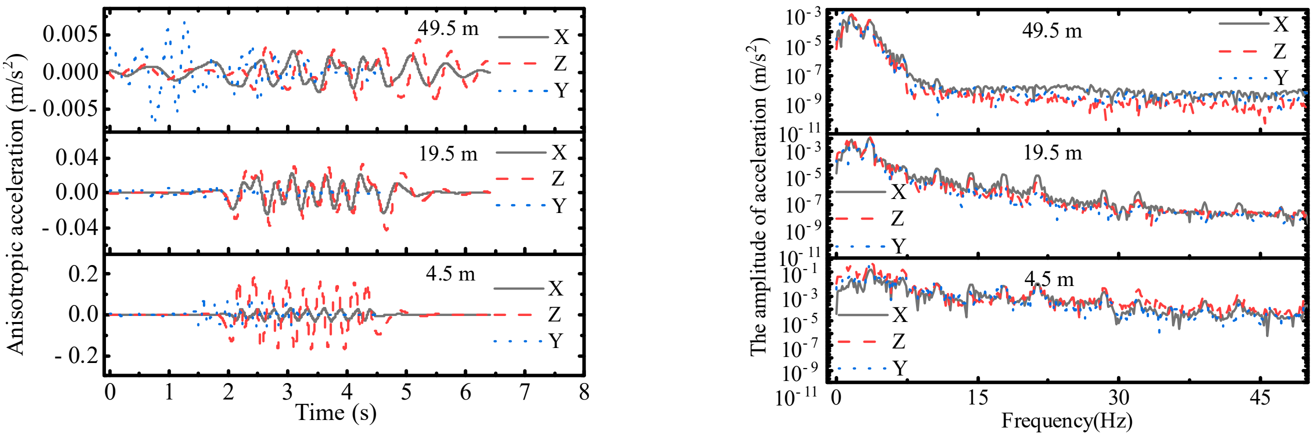

(**a**) (**b**)

Figure 16. Time history and amplitude frequency of ground three-dimensional acceleration at distances of 4.5 m, 19.5 m, and 49.5 m from the track center. (**a**) The acceleration time history. (**b**) Amplitude frequency of the acceleration.

From the perspective of acceleration curves at different distances, the short-range acceleration time history curve can better reflect the impact effect of train passing. From the perspective of the dynamic response amplitude, all dynamic response values are relatively large at close range and show a gradual attenuation as the distance to the track center increases. From the perspective of triaxial acceleration, the dynamic amplitude of the Z-direction acceleration at 4.5 m is greater than that of the other two directions. At 19.5 m, the dynamic amplitude of the X and Y directions is slightly smaller than that of the Y direction, showing a tendency to catch up. At 49.5 m, the dynamic amplitude of the X and Y directions has already exceeded that of the Z direction. In terms of the propagation speed of three-dimensional vibration waves, the acceleration in the Y direction always reaches its peak first, followed by the X direction, and the slowest in the Z direction. Moreover, the difference in the propagation velocity of the vibration wave in each direction increases with increasing distance to the center of the orbit.

2.3. Finite Element Model of the Transmission Tower-Line System

The transmission tower-line structure system is a large system composed of a series of single transmission towers and conducting (ground) lines. Previous research [36] has shown that the 'three-tower two-line system' is sufficient to meet the calculation requirements, and the calculation results are closer to the real situation. Therefore, the three-tower two-line model is also selected in this study.

2.3.1. Parameters of the Transmission Tower-Line System

The type of transmission tower is a 2A-ZM1 linear tower. The beam element is used to establish the finite element model of the transmission tower. The main parameters of the tower body are shown in Table 9. Table 10 lists the performance parameters of the established transmission conductance (ground) wire. The insulator model used in this paper is XP2-70. The tower and the ground are in a completely fixed form of restraint, and the cross arm of the transmission line, the insulator, and the conductor (ground) line are connected in a hinged manner. Finally, to make the model boundary more realistic, the insulator and conductor (ground) on both ends of the tower are restricted. The degrees of freedom of the nodes between the lines in the X direction. The finite element model of the three-tower two-line system in this section is shown in Figure 17.

Table 9. Main member parameters of the transmission tower.

Numbering	Tower Parts	Rod Specifications	Numbering	Tower Parts	Rod Specification
1	Tower leg main material	L80 × 7	8	Inner main material of upper crank arm	L45 × 4
2	Tower leg inclined material	L56 × 5	9	Outer main material of lower crank arm	L63 × 5
3	Tower leg diagonal brace	L40 × 4	10	Inner main material of lower crank arm	L56 × 5
4	Main material of tower body	L80 × 7	11	Tower leg top surface cross-section main material	L56 × 4
5	Tower body inclined material	L45 × 4, L40 × 4	12	Tower body top surface cross-section main material	L100 × 8
14	Cross-arm inclined material	L40 × 4	13	Outer main material of upper crank arm	L63 × 5
13	Cross-arm main material	L50 × 4	14	Tower body	L40 × 4

Table 10. Parameters of the transmission line.

Item	Cross-Sectional Area (mm^2)	Diameter (mm)	Line Density (kg/m)	Elastic Modulus (MPa)	Average Operating Tension (N)	Rupture Force ×0.95 (N)
LGJ—400/35	425.24	26.82	1.349	65,000	21,870	98,705
JLB40-150	148.07	15.75	0.6967	103,600	23,847	90,620

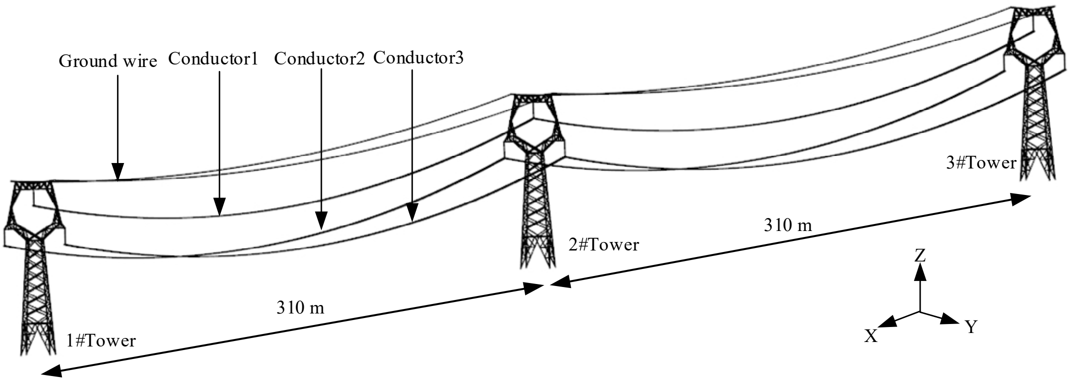

Figure 17. Finite element model of the transmission tower-line system.

2.3.2. Modal Analysis of the Transmission Tower-Line System

The interaction between transmission towers, transmission lines, and some armor clamps can affect the dynamic characteristics of individual components. Analyzing the dynamic characteristics of the tower-line coupling system is of great significance for studying the vibration characteristics of the tower-line system under vehicle-induced vibration. The partial vibration modes of the transmission tower-line structure and single transmission tower are shown in Figure 18.

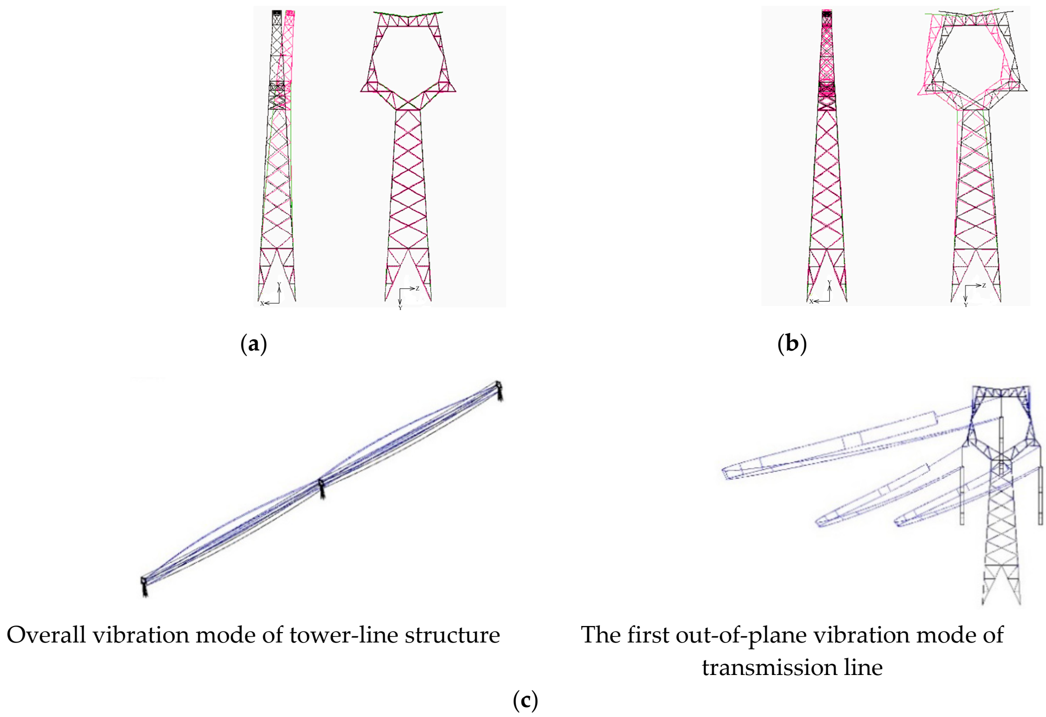

Figure 18. Partial vibration mode diagram of the transmission tower-line structure and single transmission tower. (**a**) First-order vibration mode of single tower (2.99 Hz). (**b**) Second-order vibration mode of single tower (3.73 Hz). (**c**) The first mode of vibration (0.200 Hz).

As indicated in Figure 18, the first and second natural frequencies of the transmission tower in the tower-line structure are 3.486 Hz and 3.487 Hz. Comparing the first and second natural frequencies of a single tower, it can be seen that the natural frequencies of transmission towers with tower-line structures exhibit significant amplification compared to the natural frequencies of a single transmission tower.

Ref. [40] analyzes the dynamic response of transmission towers and corresponding single towers in a tower-line system. The study shows that under the same design wind speed, the stress of the main members of the tower in the tower-line system increases more than that of the single tower. The maximum stress of the multiple members approaches or reaches the design yield strength of the steel. However, in the corresponding single tower, the stress of the members is much less than the design yield strength of the steel, and the tower remains safe. Under the same design wind speed, the member stress increase in the tower-line system is mainly caused by the vibration of the transmission lines due to the coupling effect, whereas the stress increase in the single tower is mainly caused by its self-vibration. Under a 90° wind of varying speeds, the displacement of the tower top and the stress of the main members are greater than the results of the quasistatic analysis for the corresponding single tower, demonstrating that the amplifying effect of dynamic coupling on the response of the transmission tower cannot be neglected in the tower-line system. Therefore, this article analyzes a tower-line system.

3. Results and Discussion

3.1. Working Conditions

The case where the traveling direction of the train is perpendicular to the direction of the transmission tower line (X direction) is taken as an example to study the impact of different train speeds, soil conditions, and different distances to the track on the structural vibration of the transmission tower-line system. The schematic diagram is shown in Figure 19.

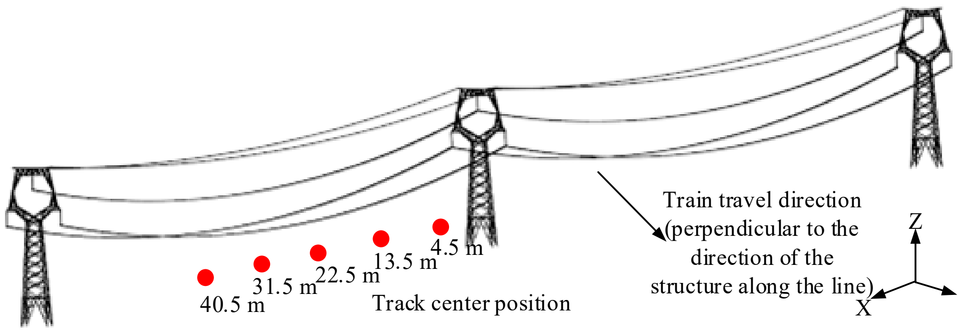

Figure 19. Schematic diagram of the train vibration source.

In this section, the soft and hard soil types introduced in Section 2 are selected, the train speed is considered to be 250 km/h, 300 km/h, 350 km/h, 400 km/h, and 450 km/h, and the distance to the track is 4.5 m, 13.5 m, 22.5 m, 31.5 m, and 40.5 m. The effective acceleration of ground vibration in the X, Y, and Z directions under different working conditions a_{rms} can be calculated by using Formula (11), and the results are shown in Figure 20.

$$a_{\mathrm{rms}} = \sqrt{a^2(t)} = \sqrt{\frac{\int_0^T a^2(t)dt}{T}} \tag{11}$$

where a_{rms} is the effective acceleration, $a(t)$ is the acceleration at different times, and T is the duration of vibration action.

Figure 20 shows that the Z direction (vertical direction) is the largest in the effective value of the three-way ground vibration acceleration, and the energy is high, especially when the distance from the center of the track is short (4.5 m~13.5 m). For the law that the effective value of ground vibration acceleration changes with the speed of the train, there is a large difference between soft and hard soil foundations. When it is a soft soil foundation, the effective ground vibration acceleration at different distances from the track has the same value with increasing train speed. For the hard soil foundation, the effective acceleration increased slowly when the train speed was lower than 350 km/h and then increased rapidly.

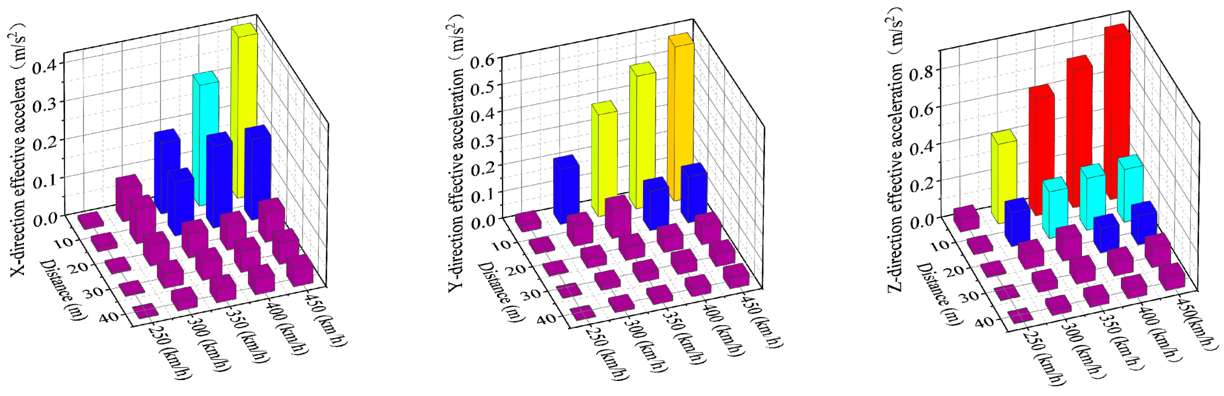

(**a**)

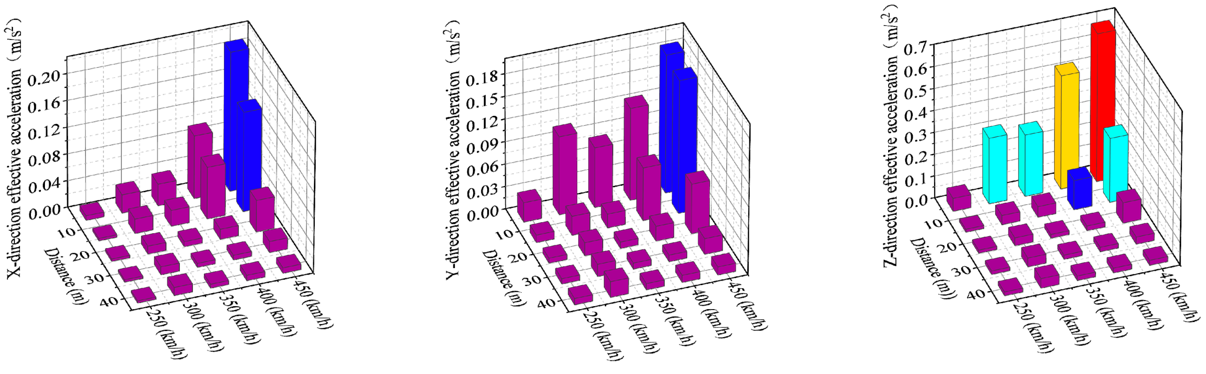

(**b**)

Figure 20. Effective acceleration under different working conditions. (**a**) Soft soil. (**b**) Hard soil.

3.2. Monitoring Points

To compare the dynamic response of the transmission tower-line structure under train-induced ground vibration for different vehicle speeds, soil qualities, and distances to the track, the axial stress of the main material of the tower legs at different heights and the displacement dynamics of the tower top in different directions under the above 50 working conditions were extracted. The monitoring points of the main material of the tower legs are shown in Figure 21a. Fifteen monitoring points evenly distributed on the main material of the tower legs are selected, and the monitoring points of the tower top displacement are shown in Figure 21b.

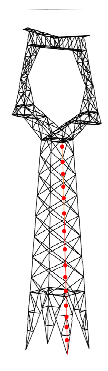

(**a**)

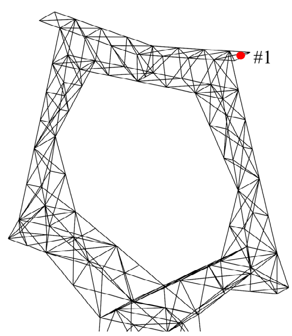

(**b**)

Figure 21. Transmission tower monitoring point diagram. (**a**) Transmission tower main material monitoring points. (**b**) Transmission tower top monitoring points.

According to the distribution law of ground vibration acceleration under the above 50 working conditions, the acceleration under various working conditions is not a simple linear distribution, and, when considering the influence of the three mixed factors of soil quality, vehicle speed, and distance, the factors that need to be considered are very complicated. Therefore, in this section, the method of controlling variables is used to analyze the dynamic response data of the transmission tower in detail. Finally, based on the dynamic response data of 50 working conditions, a three-dimensional surface diagram of the dynamic response of the transmission tower with changes in vehicle speed, soil quality, and distance is fitted.

3.3. Influence of Different Soil Qualities and Different Track Distances on the Vibration Response of the Transmission Tower-Line System

A speed of 250 km/h is taken as the control variable, and the dynamic response of the tower top displacement and the main material stress under the condition of a speed of 250 km/h are analyzed, which is affected by the soil and the distance to the track. From the modal analysis of the transmission tower-line structure in Section 2.3.2, it can be seen that the main mode shape of the transmission tower that appears for the first time is that the transmission tower bends in the X direction (in-plane), which is consistent with the bending direction of the first-order mode shape of the single transmission tower. This shows that the in-plane stiffness of the transmission tower is smaller, and it is more susceptible to the influence of ground vibration. The Y direction is greatly affected by the transmission conductor (ground) line. Therefore, the following analysis mainly focuses on the X direction and Y direction ground acceleration time-history data and frequency domain data, as shown in Figures 22 and 23. When the vehicle speed is 250 km/h, the X-direction acceleration amplitude corresponding to the soft soil foundation is obviously larger than that of the hard soil foundation. However, with the increase in the distance to the track, the X-direction acceleration decay rate corresponding to the hard soil foundation is significantly larger than that of the soft soil foundation. As shown in the X-direction acceleration amplitude-frequency diagrams of the two sites, the acceleration frequency is mainly within 10 Hz, and the main frequencies of both are relatively close to the first-order natural vibration frequency (2.99 Hz) of the single transmission tower. However, in terms of the frequency domain energy distribution of soft and hard soils, the vibration acceleration of the hard soil foundation accounts for a significant proportion near the fundamental frequency of the transmission tower, which is larger than that of the soft soil type. Due to the presence of wheels, the peaks of the acceleration time history undergo periodic changes. At a speed of 250 km/h, the peak value of the X direction appears at a distance of 13.5 m from the track in Figure 22, indicating that the energy in the soft soil foundation is highest here, while the peak value of hard soil occurs at 4.5 m. The peak values of both soil types under the Y direction appear at 4.5 m, indicating that the highest energy of the Y component is at 4.5 m for both soil types. In Figure 23, the peak values of soft soil and hard soil appear at 13.5 m and 4.5 m, respectively, corresponding to Figure 22. From the acceleration time history data and amplitude frequency data in the Y direction, there is a certain difference between the Y direction and the X direction. As far as the acceleration amplitude level is concerned, there is a slight difference between the two, and the acceleration response amplitude under soft soil is also significantly greater than that of hard soil. The frequency domain energy distribution in the Y direction is basically the same as that in the X direction, but at high frequencies, the energy is slightly larger than that in the X direction.

Incorporating the time history, consider the effective displacement of the tower's top in the X and Y directions. It can be determined by Formula (12):

$$u_{\mathrm{rms}} = \sqrt{u^2(t)} = \sqrt{\frac{\int_0^T u^2(t)dt}{T}} \tag{12}$$

where u_{rms} is the effective displacement, $u(t)$ is the displacement at different times, and T is the duration of vibration action. By Formula (12), the effective displacement values of the tower top with different soil qualities and different distances from the track can be obtained, as shown in Table 11 and Figure 24.

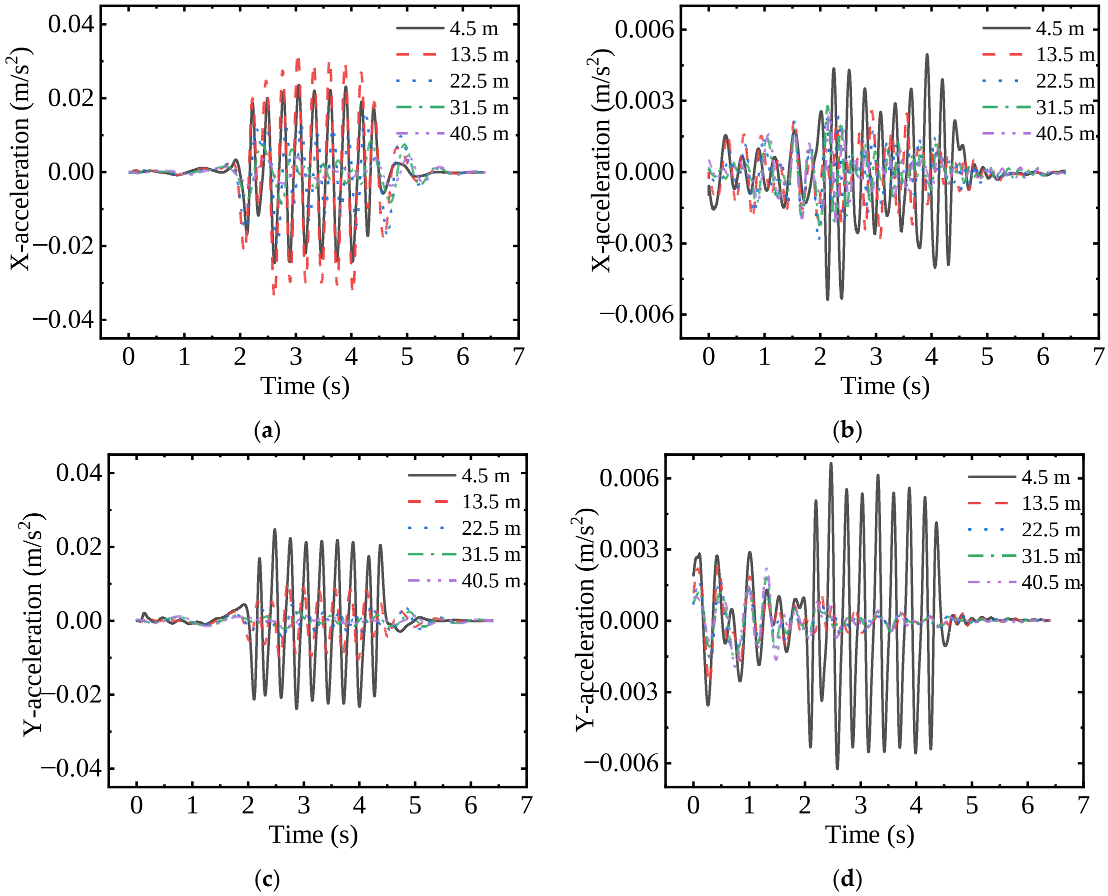

Figure 22. The X- and Y-direction acceleration time history diagram from 250 km/h to different distances from the track center. (**a**) Soft soil foundation. (**b**) Hard soil foundation. (**c**) Soft soil foundation. (**d**) Hard soil foundation.

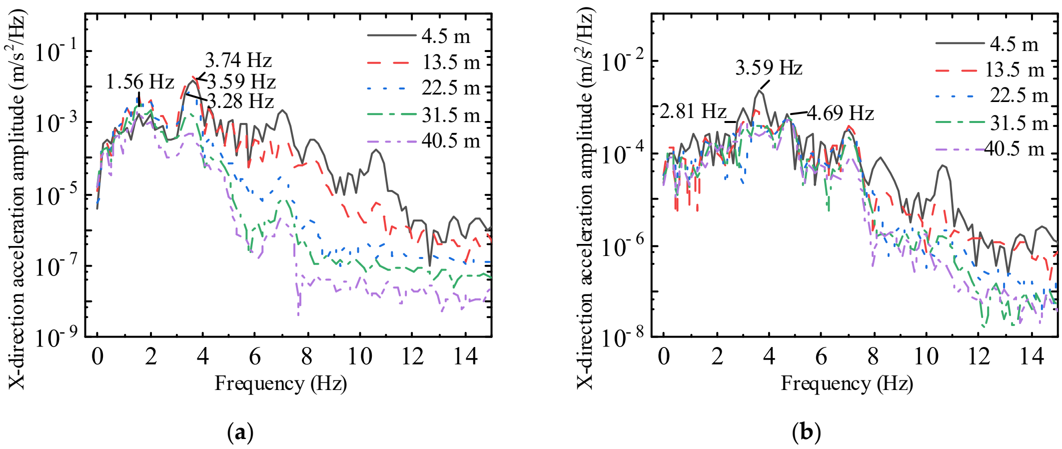

Figure 23. *Cont.*

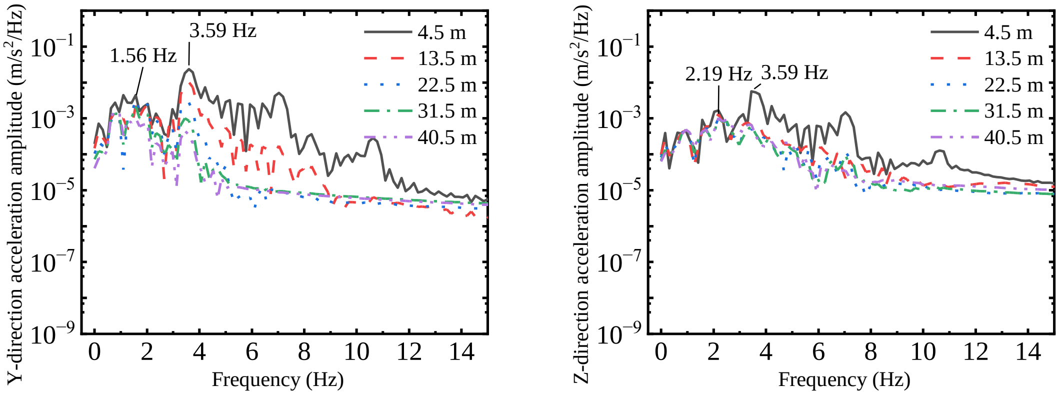

(**c**) (**d**)

Figure 23. The X- and Y-direction acceleration amplitude-frequency diagram at different distances from the track center at 250 km/h. (**a**) Soft soil foundation. (**b**) Hard soil foundation. (**c**) Soft soil foundation. (**d**) Hard soil foundation.

Table 11. Effective displacement of the tower top at different distances.

Distance to Track (m)	Soft Soil X-Direction u_{rms} (mm)	Soft Soil Y-Direction u_{rms} (mm)	Hard Soil X-Direction u_{rms} (mm)	Hard Soil Y-Direction u_{rms} (mm)
4.5 m	4.07	0.56	3.49	2.46
13.5 m	4.25	0.66	4.06	2.16
22.5 m	4.25	0.84	4.17	1.75
31.5 m	4.23	0.98	3.51	1.57
40.5 m	3.03	0.90	3.44	1.48

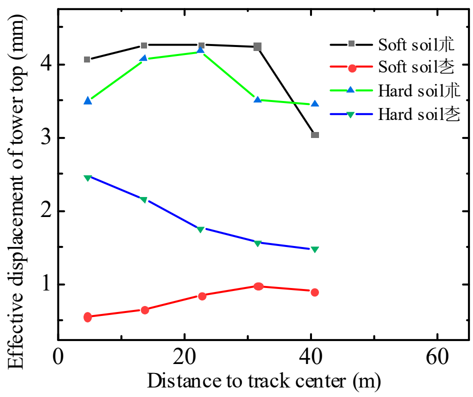

Figure 24. Effective displacement value of the tower top.

From the change trend of the effective displacement of the tower top with the distance from the track, the change trend of the effective displacement in the X direction is basically the same as the change law of the effective value of the ground vibration acceleration in the X direction, which increases first and then decreases, which is particularly evident in the case of soft soil foundation soil. The change trend of the tower top displacement in the X direction under the hard soil type foundation soil is in poor agreement with the change trend of the effective value of the ground X-direction vibration acceleration, which is mainly due to the use of a three-way ground vibration input in the excitation of the transmission tower-line system in this section. The ground vibration input in the direction is affected by the ground vibration in other directions, so it is different. From the overall displacement response, when the distance from the track center is greater than 13.5 m, all the effective displacements decrease except the Y-direction displacement of the soft soil type foundation. From the point of view of the effective displacement value of the tower top, at a close distance (4.5 m), the acceleration amplitude of hard soil is greater than that of soft soil, so the effective displacement of the top of the tower under hard soil is also greater than that of soft soil. However, due to the different Rayleigh wave velocities of the two soils, the Rayleigh wave velocity corresponding to the soft soil foundation soil is obviously smaller than that of the hard soil foundation soil; therefore, at a relatively long distance (40.5 m), the effective displacement value of the tower top under soft soil is significantly greater than that of hard soil.

To compare the stress response changes of the transmission tower under different working conditions, the stress data of the main material unit marked in Figure 21a are extracted, and Figures 25 and 26 draw the maximum axial tension and compression stress diagram of the unit with the height of the tower. The maximum tensile stress of the main material is mainly distributed in the tower body 12 m height, and the maximum compressive stress is mainly distributed in the tower body 8 m. The maximum tensile stress of the main material in the hard soil type foundation soil decreases with the increase in the orbital distance as a whole, which is almost consistent with the change law of ground vibration acceleration, which corresponds to the decrease in the consistency of soft soil type foundation soil.

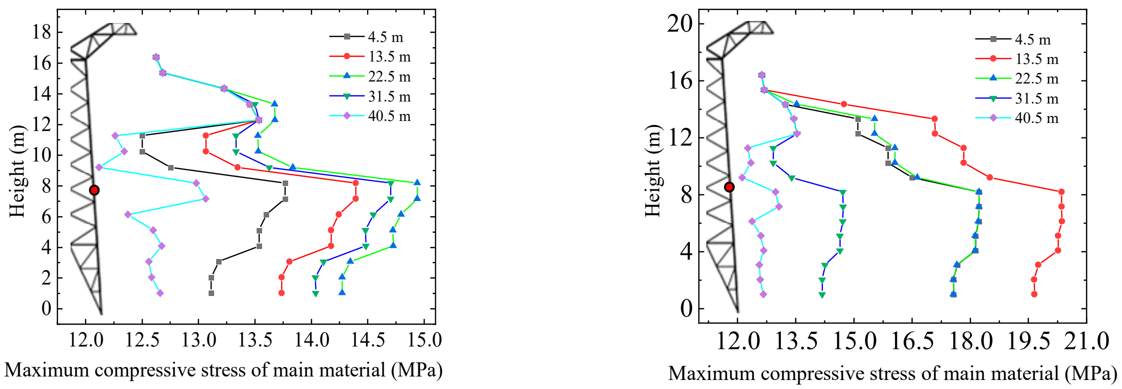

(**a**) (**b**)

Figure 25. The maximum compressive stress distribution of the main material at different distances from the track center at 250 km/h. (**a**) Soft soil. (**b**) Hard soil.

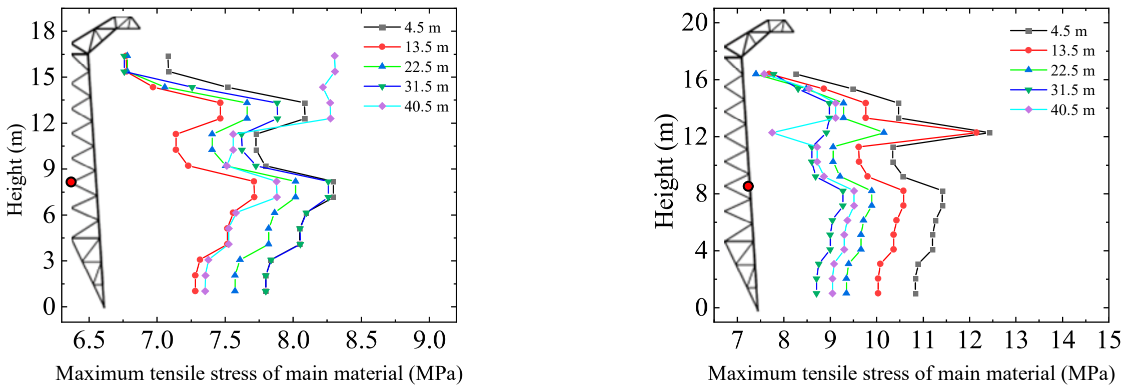

(**a**) (**b**)

Figure 26. The maximum tensile stress distribution of the main material at different distances from the track center at 250 km/h. (**a**) Soft soil. (**b**) Hard soil.

3.4. Influence of Different Train Speeds on the Vibration Response of the Transmission Tower-Line System

From the conclusion of the previous section, when the train speed is 250 km/h, the dynamic response of the transmission tower-line structure is the largest at a distance of 13.5 m from the center of the track. The following is to study the influence of different vehicle speeds on the dynamic response of the transmission tower-line structure under the environmental vibration caused by the train. In this section, the distance to the track is used as the control variable, and the 13.5 m influence of different train speeds on the dynamic response of the structure. Figures 27 and 28 show the time-history and amplitude-frequency diagrams of the ground X-direction acceleration under the two soil conditions at different train speeds down to track 13.5 m.

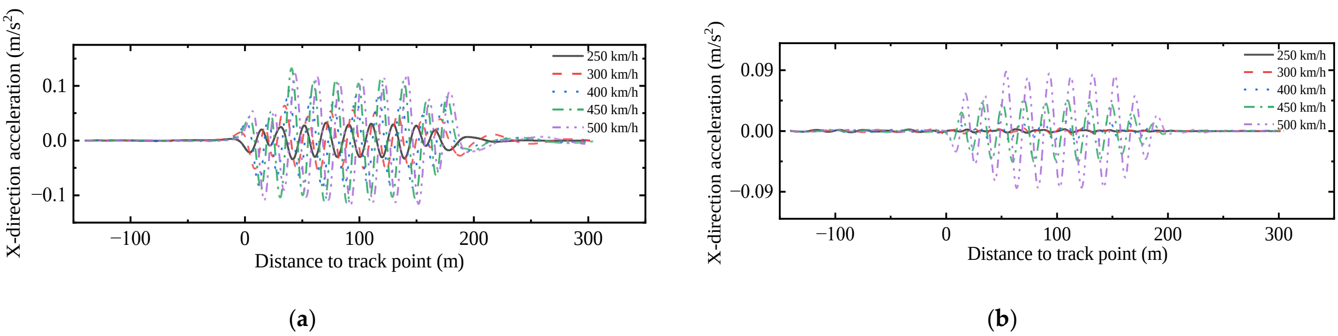

Figure 27. X-direction acceleration time history response at 13.5 m under soft and hard soil at different speeds. (**a**) Soft soil foundation. (**b**) Hard soil foundation.

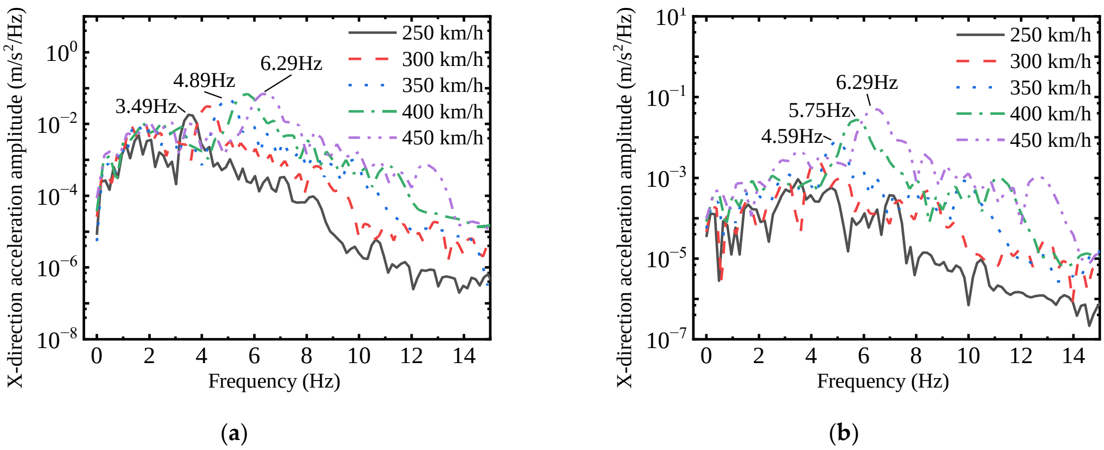

Figure 28. X-direction acceleration amplitude-frequency diagram at 13.5 m under soft and hard soil at different speeds. (**a**) Soft soil foundation. (**b**) Hard soil foundation.

Judging from the acceleration time-history data in the X direction, the acceleration amplitude corresponding to the soft soil type foundation soil is slightly larger than that of the hard soil type foundation soil; the acceleration amplitude in the X direction under both soil conditions increases with increasing vehicle speed, but the acceleration amplitude under the two soil conditions varies with the speed of the vehicle. The acceleration amplitude corresponding to the soft soil is faster at first and then slower, while the acceleration amplitude under the hard soil is gradually accelerated. In addition, from the analysis of the acceleration amplitude-frequency data in the two fields, with increasing vehicle speed, the frequency component of the acceleration gradually approaches the high-frequency section, which gradually moves away from the fundamental frequency of the transmission tower. The frequency component of the acceleration at the minimum vehicle speed is close to the high frequency of the transmission tower and gradually moves away as the vehicle speed increases.

Previous results showed that the Z-direction displacement fluctuation of the top of the transmission tower is small, and the response difference under different working conditions is also small. Therefore, only details of the X- and Y-direction displacements of the transmission tower are analyzed and compared in this section. The effective displacement of the tower top in the X and Y directions under different soil qualities corresponding to the vehicle speed needs to be calculated by using Formula (12). The results are shown in Table 12 and Figure 29.

Table 12. Effective displacement of the tower top under different train speeds.

Train Speed (km/h)	Soft Soil X-Direction u_{rms} (mm)	Soft Soil Y-Direction u_{rms} (mm)	Hard Soil X-Direction u_{rms} (mm)	Hard Soil Y-Direction u_{rms}
250	4.25	0.70	3.37	0.92
300	3.08	0.72	3.21	1.00
350	10.10	2.22	10.00	3.47
400	3.16	0.70	3.02	1.15
450	3.37	0.66	4.06	2.16

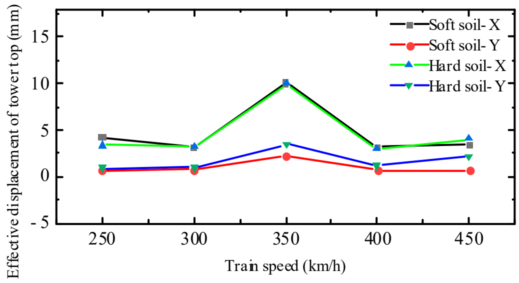

Figure 29. Effective tower top displacement at different speeds up to 13.5 m on the track.

As shown in Figure 29, when the speed is less than 450 km/h, the displacement in the X direction of the transmission tower is always greater than the displacement in the Y direction, which is mainly due to the weak stiffness of the transmission tower in the X direction. Under the ground vibration caused by the vehicle, the transmission tower does not increase linearly with increasing train speed but has a speed that has the greatest influence (350 km/h), mainly because the factors affecting the dynamic response of the structure are not only the amplitude of the time history acceleration but also the duration and frequency components of the ground vibration. Figure 28 shows from the amplitude-frequency diagram of the Y-direction acceleration of the middle ground that with increasing train speed, the main frequency range of the ground vibration gradually approaches the higher frequency band, and the difference between this and the fundamental frequency of the transmission tower will gradually increase. The ground vibration duration acting on the transmission tower-line structure will gradually decrease, so even if the vehicle-induced ground vibration acceleration amplitude will increase with increasing vehicle speed, the dynamic response of the structure will not show a linear increasing trend. Overall, due to the duration and frequency distribution of ground vibration, the effective displacement values of the tower top in the X direction and Y direction under the two kinds of soil are the largest at 350 km/h, which are 10.10 mm and 10.00 mm, respectively.

To compare the stress response changes of the main material of the transmission tower under different vehicle speeds, the main material element stress data marked in Figure 21a are extracted, and Figures 30 and 31 show the maximum axial tensile and compressive stresses of the element with the change in tower height.

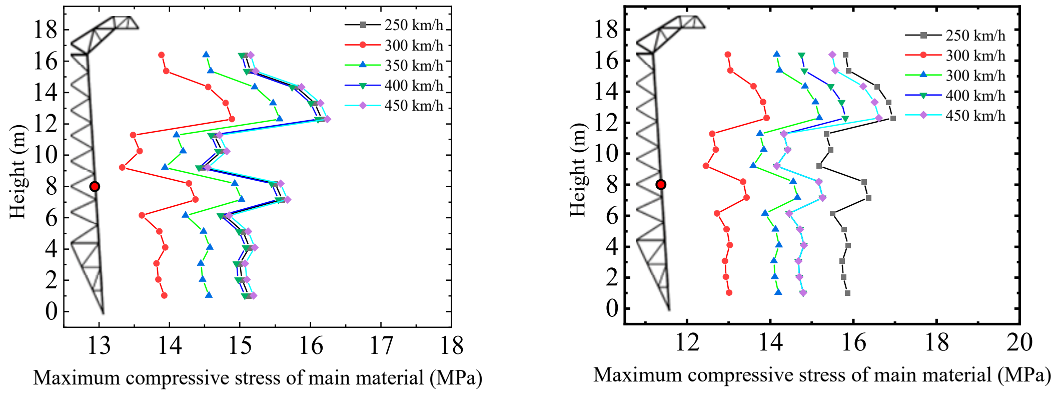

(**a**) (**b**)

Figure 30. The maximum compressive stress of the main material is distributed along the height at different speeds. (**a**) Soft soil foundation. (**b**) Hard soil foundation.

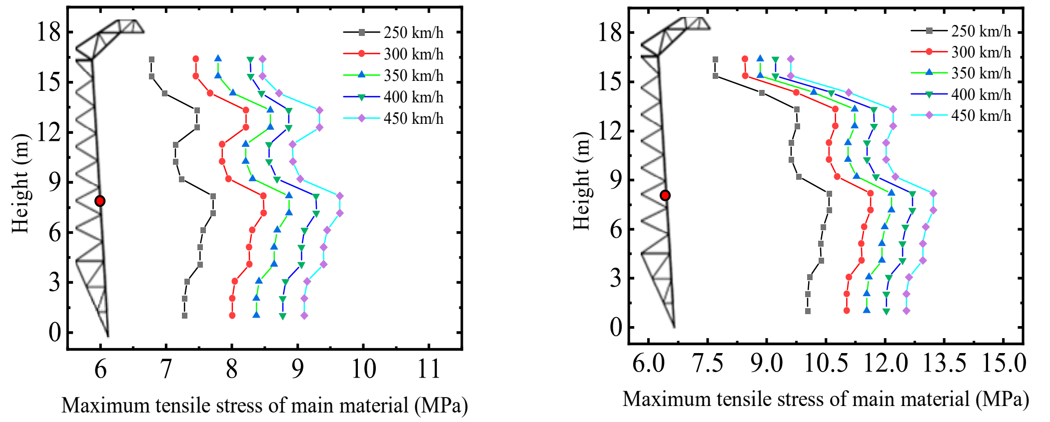

(**a**) (**b**)

Figure 31. The maximum tensile stress of the main material at different speeds was distributed along the height. (**a**) Soft soil foundation. (**b**) Hard soil foundation.

From the data of the maximum tensile and compressive stress along the height of the main material of the transmission tower in Figures 30 and 31, the trend of the stress along the height is basically the same, and the maximum value of the tensile stress gradually increases with the speed of the vehicle, but the growth rate is first fast and then slow, while the compressive stress is the highest. The value as a whole satisfies the linear increasing trend with the vehicle speed.

The above control variables are used to compare the dynamic response differences of the top displacement of the transmission tower and the stress of the main material of the tower body at different vehicle speeds, soil qualities, and different distances from the track. To provide a more detailed analysis of the response changes of transmission towers at different soil types, vehicle speeds, and distances from the track, taking the tower top displacement that is greatly affected by ground vibration as an example, Formula (12) is used to analyze its effective values throughout the time domain, and the effective displacements of the tower top in the X and Y directions are fitted to obtain a three-dimensional curved surface, as shown in Figure 32.

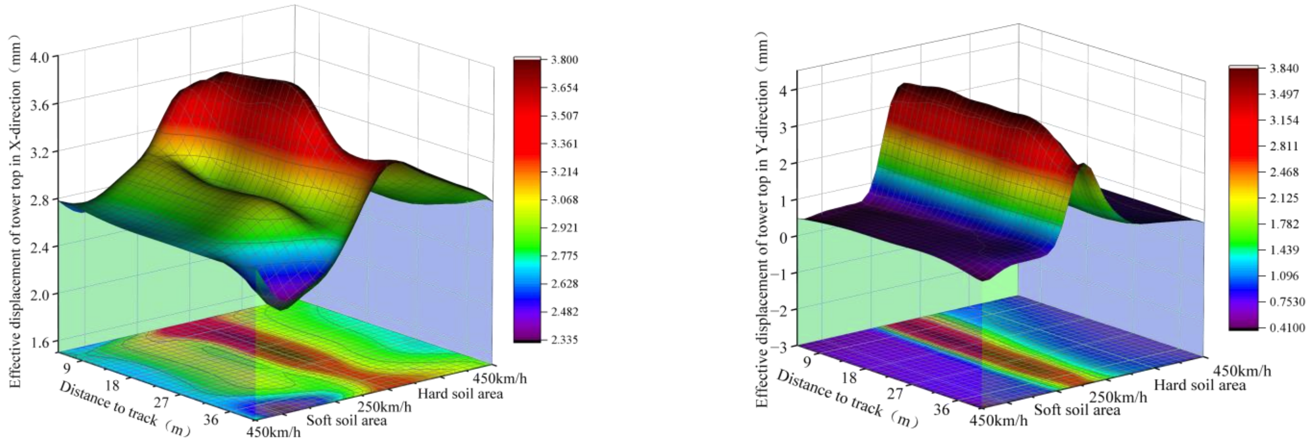

(**a**) (**b**)

Figure 32. Transmission tower top displacement effective value fitting diagram. (**a**) Data fitting of effective displacement of tower top in X direction. (**b**) Data fitting of effective displacement of tower top in Y direction.

Figure 32 indicates that under the ground vibration caused by the train, the displacement of the transmission tower in the Y direction is affected by the speed of the train more than the displacement in the X direction. At 250 km/h, the dynamic response of the tower top displacement in the X and Y directions is very small. With increasing train speed, the change in the tower top displacement in the X direction is small, while the tower top displacement in the Y direction is almost exhausted quickly. This explains why the stiffness of the transmission tower-line system in-plane is small and is greatly affected by ground vibration. In addition, the displacement of the top of the tower at different distances from the track at the same speed is generally attenuated, but there is a trend of increasing first and then decreasing. From the three-dimensional surface map, it can be seen that the transmission tower line is greatly affected by the ground vibration in the range of 4.5 m~30 m from the track.

The effective value of ground vibration acceleration caused by high-speed trains increases with increasing vehicle speed and decreases with increasing distance to the track. However, the dynamic response corresponding to the transmission tower-line system is not so, which is affected by the frequency distribution, acceleration amplitude and vibration holding time of ground vibration. From the three-dimensional surface diagram, it can be concluded that the load holding time and frequency distribution occupy the main influence, and from the figure can be a more intuitive conclusion. The train speed with a greater influence is 250 km/h~350 km/h, and the transmission tower-line system has the most obvious response in the range of 4.5~30 m to the track.

For further analysis, the transfer function of the displacement of the foundation soil to the displacement of the tower top in the X direction and Y direction at 22.5 m under soft soil at 250 km/h are presented in Figure 33. As seen from Figure 33, the overall amplitude levels of the X direction and Y direction are similar, which can also be observed from the effective displacement value of the top of the tower. In addition, the frequency range of higher amplitude is mainly within 2~4 Hz, which is close to the first two natural frequencies of the transmission tower. The peaks of the transfer function in the X and Y directions occur at 2.99 Hz and 3.73 Hz, which is consistent with the first two mode shapes of the transmission tower shown in Figure 18. Overall, the amplitude of the transfer function in the fundamental frequency range of the tower is relatively high, showing an obvious amplification phenomenon. This also indicates that the vibration of the tower is sensitive in this frequency range (2~4 Hz).

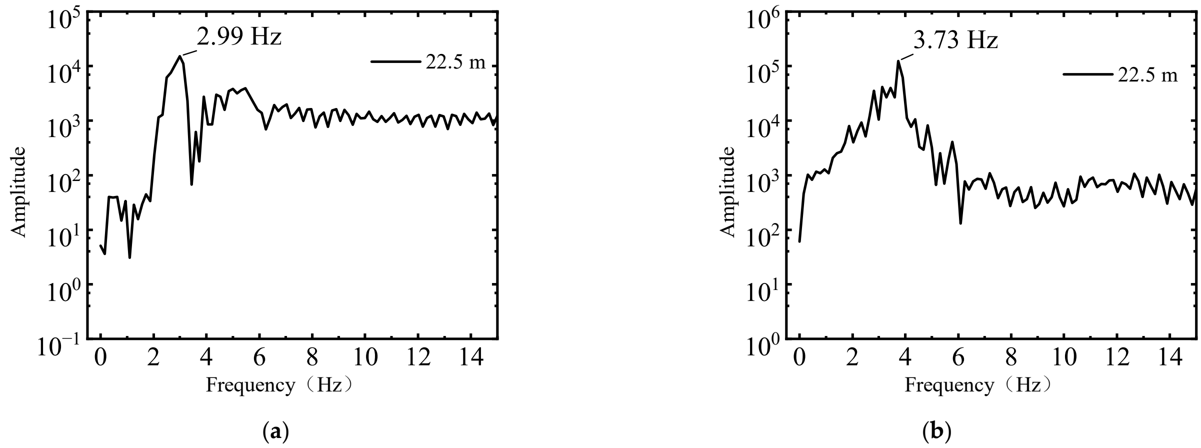

Figure 33. Transfer function of the displacement at the top of the tower response under a soft soil foundation. (**a**) Transfer function of X-direction displacement response at the top of the tower. (**b**) Transfer function of Y-direction displacement response at the top of the tower.

4. Conclusions

In this study, the commonly used ICE3 train and 220 kV typical transmission tower-line structure are used as the research objects, and the method of numerical simulation is used to study the impact of ground vibration generated by the train on the structure of the transmission tower line when the high-speed train crosses the transmission line. The influence of the train running speed, soil conditions and transmission tower-to-track distance on the dynamic response of the tower-line structure under the action of vehicle-induced ground vibration is analyzed and discussed. The main conclusions are as follows:

(1) The ground vibration characteristics of trains are mainly influenced by factors such as track irregularity, soil quality, and train speed. The irregularity of the track has a significant impact on the vibration response of structures near the track, and considering the irregularity of the track, the high-frequency components in the roadbed response are significantly higher than those in the smooth state. The roadbed structure also has a great inhibitory effect on high-frequency vibration at the vibration source, and the attenuation of vibration waves through the roadbed structure to the ground surface vibration beyond 4.5 m of the track can be ignored due to the influence of track irregularity. The soil quality of a free field has a significant impact on vehicle-induced surface vibration: the amplitude of the vehicle-induced vibration response on the surface corresponding to a soft soil foundation is significantly greater than that of hard soil, while the frequency distribution of ground vibration on a hard soil foundation is wider than that on soft soil. The vibration response amplitude of the ground surface increases significantly with increasing vehicle speed, but with increasing vehicle speed, the impact effect of wheel sets on the ground surface near the source gradually weakens;

(2) The predominant frequency of the acceleration responses of the transmission tower under soft and hard soil foundations is mainly within 10 Hz, and the main frequency of both is close to the first-order natural frequency (2.99 Hz) of a single transmission tower. The tower-line structure vibrates mainly in the low-frequency range, and the vibration of trains is distributed in a wide frequency range. The amplitude of the high-level displacement response transfer function of the X-direction and Y-direction tower tops is concentrated in the range of 2~4 Hz. This indicates that the vibration of the tower is sensitive in this frequency range. In addition, the effective displacement along the top of the tower (X direction) is greater than the dynamic response in the vertical direction (Y direction);

(3) The effective value of ground vibration acceleration caused by trains will increase with increasing train speed and decrease with increasing distance to the track. Due

to the influence of various factors, such as the frequency distribution, acceleration amplitude, and vibration duration of ground vibration, the dynamic response of the transmission tower-line system is not the same. From the point of view of the effective displacement value of the tower top, when the speed is 350 km/h, the effective displacement value of the tower top under the two kinds of soil is the largest. At a close distance (4.5 m), the acceleration amplitude of hard soil is greater than that of soft soil, so the effective displacement of the top of the tower under hard soil is also greater than that of soft soil. However, due to the different Rayleigh wave velocities of the two soils, the Rayleigh wave velocity corresponding to the soft soil foundation soil is obviously smaller than that of the hard soil foundation soil; therefore, at a relatively long distance (40.5 m), the effective displacement value of the tower top under soft soil is significantly greater than that of hard soil. Overall, for the crossing areas of the soft soil foundation soil in this article, the vibration response of the transmission tower is the highest when the train speed is 250~400 km/h and the distance to the track is within 40 m. The transmission tower in the crossing section of hard soil foundation soil has the highest vibration response when the train speed is 250~350 km/h and the distance to the track is within 30 m.

Author Contributions: Conceptualization, G.Z. and M.Z.; methodology, G.Z., M.W. and Y.L.; software, G.Z. and M.Z.; validation, M.W., Y.L. and G.Z.; formal analysis, M.W. and Y.L.; investigation, Y.L. and M.Z.; resources, M.Z.; data curation, M.W.; writing—original draft preparation, G.Z., M.W. and Y.L.; writing—review and editing, G.Z., Y.L. and M.Z. All authors have read and agreed to the published version of the manuscript.

Funding: This work was sponsored by the Natural Science Foundation of Henan (grant no. 222300420549) and the Cultivating Fund Project for Young Teachers of Zhengzhou University (grant no. JC21539028).

Data Availability Statement: Data are contained within this article.

Conflicts of Interest: The authors declare no conflict of interest.

References

1. We, Y. Preface: Current research progress on mechanics of high-speed rail. *J. Mech. Engl. Ed.* **2014**, *30*, 846–848. [CrossRef]
2. Jia, Y.Y. *Research on Vibration Source Model and Ground Vibration Response of Subway Train*; Science and Technology Literature Publishing House: Beijing, China, 2016.
3. Timoshenko, S.P. Method of analysis of statical and dynamical stresses in rail. *J. Phys. Soc. Jpn.* **1927**. [CrossRef]
4. Jenkins, H.H.; Stephenson, J.E.; Clayton, G.A.; Morland, G.W.; Lyon, D. The effect of track and vehicle parameters on wheel/rail vertical dynamic loads. *J. Railw. Eng. Soc.* **1974**, *3*, 2–16.
5. Ditzel, A.; Herman, G.C.; Drijkoningen, G.G. Seismograms of moving trains: Comparison of theory and measurements. *J. Sound Vibr.* **2001**, *248*, 635–652. [CrossRef]
6. Kaynia, A.M.A.; Madshus, C.A.; Zackrisson, P.B. Ground vibration from high-speed trains: Prediction and countermeasure. *J. Geotech. Geoenviron. Eng.* **2000**, *126*, 531–537. [CrossRef]
7. Sheng, X.S.X.; Jones, C.J.C.; Thompson, D.T.D. A theoretical model for ground vibration from trains generated by vertical track irregularities. *J. Sound Vibr.* **2004**, *272*, 937–965. [CrossRef]
8. Hayakawa, K.; Sawatake, M.; Gotoh, R.; Matsui, T. Reduction effect of ballast mats and eps blocks on ground vibration caused by trains and its evaluation. In *INTER-NOISE and NOISE-CON Congress and Conference Proceedings*; Institute of Noise Control Engineering: Washington, DC, USA, 1992; pp. 593–596.
9. Xia, H.; Cao, Y.M.; De Roeck, G. Theoretical modeling and characteristic analysis of moving-train induced ground vibrations. *J. Sound Vibr.* **2010**, *329*, 819–832. [CrossRef]
10. Erkal, A.; Kocagoz, M.S. Interaction of vibrations of road and rail traffic with buildings and surrounding environment. *J. Perform. Constr. Facil.* **2020**, *34*, 04020038. [CrossRef]
11. Motazedian, D.; Hunter, J.A.; Sivathayalan, S.; Pugin, A.; Pullan, S.; Crow, H.; Banab, K.K. Railway train induced ground vibrations in a low V_s soil layer. *Soil Dyn. Earthq. Eng.* **2012**, *36*, 1–11. [CrossRef]
12. Niu, D.X.; Deng, Y.H.; Mu, H.D.; Chang, J.; Xuan, Y.; Cao, G. Attenuation and propagation characteristics of railway load-induced vibration in a loess area. *Transp. Geotech.* **2022**, *37*, 100858. [CrossRef]
13. Chen, J.; Han, T.; Yu, X.; Cao, Y. Experiment study on dynamic responses of bridge and surrounding environment induced by high-speed trains. In Proceedings of the 2010 WASE International Conference on Information Engineering, Washington, DC, USA, 14–15 August 2010.

14. Hesami, S.; Ahmadi, S.; Ghalesari, A.T. Numerical modeling of train-induced vibration of nearby multi story building: A case study. *KSCE J. Civ. Eng.* **2016**, *20*, 1701–1713. [CrossRef]
15. Zhou, Y.; Wang, B. Dynamic analysis of building vibration induced by train along railways. *J. Vib. Shock* **2006**, *25*, 36–41.
16. Celebi, E.; Kirtel, O.; Istegun, B.; Zulfikar, A.C.; Goktepe, F.; Faizan, A.A. In situ measurements and data analysis of environmental vibrations induced by high-speed trains: A case study in northwestern turkey. *Soil Dyn. Earthq. Eng.* **2022**, *156*, 107211. [CrossRef]
17. Schaumann, M.; Gamba, D.; Guinchard, M.; Scislo, L.; Wenninger, J. Effect of ground motion introduced by hl-lhc ce work on lhc beam operation. In Proceedings of the 10th International Particle Accelerator Conference, Melbourne, Australia, 19–24 May 2019; p. THPRB116.
18. Schaumann, M.; Gamba, D.; Garcia Morales, H.; Corsini, R.; Guinchard, M.; Scislo, L.; Wenninger, J. The effect of ground motion on the lhc and hl-lhc beam orbit. *Nucl. Instrum. Methods Phys. Res. Sect. A Accel. Spectrometers Detect. Assoc. Equip.* **2023**, *1055*, 168495. [CrossRef]
19. Farahani, M.V.; Sadeghi, J.; Jahromi, S.G.; Sahebi, M.M. Modal based method to predict subway train-induced vibration in buildings. *Structures* **2023**, *47*, 557–572. [CrossRef]
20. Davenport, A.G. Gust response factors for transmission line loading. In *Wind Engineering*; Cermak, J.E., Ed.; Elsevier: Pergamon, Turkey, 1980; pp. 899–909.
21. Zhao, S.; Yan, Z.; Li, Z.; Dong, J.; Zhong, Y. Investigation on wind tunnel tests of an aeroelastic model of 1000 kv sutong long span transmission tower-line system. *Proc. Chin. Soc. Electr. Eng.* **2018**, *38*, 5257–5265.
22. Li, Z.L.; Hu, Y.J.; Tu, X. Wind-induced response and its controlling of long-span cross-rope suspension transmission line. *Appl. Sci.* **2022**, *12*, 1488. [CrossRef]
23. Yang, F.; Zhang, H.; Wang, F.; Huang, G. Gust response coefficients of transmission line conductor. *J. Vib. Shock* **2021**, *40*, 85–91.
24. Wang, L.; Yao, Y.; Zhang, Y.; Huang, J. Ice-shedding and breaking force analysis of transmission tower line system under different icing conditions. *Ind. Constr.* **2019**, *49*, 7–12.
25. Xue, J.Y.; Mohammadi, F.; Li, X.; Sahraei-Ardakani, M.; Ou, G.; Pu, Z.X. Impact of transmission tower-line interaction to the bulk power system during hurricane. *Reliab. Eng. Syst. Saf.* **2020**, *203*, 107079. [CrossRef]
26. Feng, H.F.; Wang, Y.R. Research on safety and reliability of overhead transmission lines across high-speed railway lines design. *Electr. Plat. Railr.* **2020**, *31*, 30–32.
27. Yin, M.; He, Z.H.; Zhang, Y.C.; Liu, Y.C.; Yang, J.; Zhang, Z.Y. Dynamic response of transmission lines crossing high-speed railway. *IEEE Trans. Power Deliv.* **2022**, *37*, 2143–2152. [CrossRef]
28. Zhang, M.; Liu, Y.; Liu, H.; Zhao, G.F. Dynamic response of an overhead transmission tower-line system to high-speed train-induced wind. *Wind Struct.* **2022**, *34*, 335–353.
29. Liu, H. Analysis of the Influence of Train Wind on the Transmission Tower-Line Structure across High-Speed Railway. Master's Thesis, Zhengzhou University, Zhengzhou, China, 2021.
30. Wang, F.X. Numerical Simulation and Vibration Characteristics Analysis of Environmental Vibration of High-Speed Railway Based on ABAQUS. Master's Thesis, Beijing Jiaotong University, Beijing, China, 2014.
31. Chen, X.M.; Wang, L.; Tao, X.X. Research on the evaluation method of track regularity of trunk railway in China. *China Railw. Sci.* **2008**, *29*, 21–27.
32. Xu, L.; Chen, X.M.; Jia, H.B. Power spectrum analysis of track irregularity for 350 km/h Shanghai-Nanjing passenger dedicated line. *J. Civ. Eng. Manag.* **2013**, *30*, 22–26.
33. Qiu, G.D. Research on Train Vibration Response Based on Track Random Irregularity. Master's Thesis, South China University of Technology, Guangzhou, China, 2014.
34. Chen, G.; Zhai, W.M. Numerical simulation of random process of railway track irregularity. *J. Southwest Jiaotong Univ.* **1999**, *34*, 13–17.
35. *TB10621-2014*; Code for Design of High-Speed Railway. China Railway Publishing House: Beijing, China, 2019.
36. Liu, Y. *Basic Principles of Soil Dynamics*; Tsinghua University Press: Beijing, China, 2019.
37. Clough, R.W.; Penzien, J. *Dynamics of Structures*; McGraw-Hill: New York, NY, USA, 1975.
38. Han, H.Y. Numerical Simulation Analysis of Ground Vibration Caused by High-Speed Trains on Soft Soil Subgrade. Master's Thesis, Southwest Jiaotong University, Chengdu, China, 2012.
39. Zhang, L.L. Random Wind Field Research and Wind-Resistant Reliability Analysis of High-Rise and High-Rise Structures. Doctoral Thesis, Tongji University, Shanghai, China, 2006.
40. Zhang, M.; Zhao, G.; Wang, L.; Li, J.; Ma, X. Wind-induced coupling vibration effects of high-voltage transmission tower-line systems. *Shock Vib.* **2017**, *2017*, 1205976. [CrossRef]